

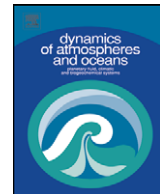


ELSEVIER

Contents lists available at ScienceDirect

## Dynamics of Atmospheres and Oceans

journal homepage: [www.elsevier.com/locate/dynatmoce](http://www.elsevier.com/locate/dynatmoce)



# Air–sea interaction over ocean fronts and eddies

R.J. Small<sup>a,j,\*</sup>, S.P. deSzeoke<sup>a,b</sup>, S.P. Xie<sup>a,c</sup>, L. O'Neill<sup>d,k</sup>, H. Seo<sup>e,f</sup>,  
Q. Song<sup>d,g</sup>, P. Cornillon<sup>g</sup>, M. Spall<sup>h</sup>, S. Minobe<sup>i</sup>

<sup>a</sup> International Pacific Research Center, POST 401, 1680 East-West Road, University of Hawaii, Honolulu, HI 96822, USA

<sup>b</sup> NOAA/ESRL/PSD3, 325 Broadway, Boulder, CO 80304, USA

<sup>c</sup> Department of Meteorology, HIG350, School of Ocean and Earth Science and Technology,  
2525 Correa Road, University of Hawaii, Honolulu, HI 96822, USA

<sup>d</sup> College of Oceanic and Atmospheric Sciences, Oregon State University, 104 COAS Admin. Building,  
Corvallis, OR 97331-5503, USA

<sup>e</sup> Climate Research Division, Scripps Institution of Oceanography, La Jolla, CA 92093-0224, USA

<sup>f</sup> Department of Atmospheric and Oceanic Sciences, UCLA, 7127 Math Sciences Building,  
405 Hilgard Avenue, Los Angeles, CA 90095-1565, USA

<sup>g</sup> Graduate School of Oceanography, University of Rhode Island, Narragansett, RI 02882, USA

<sup>h</sup> Department of Physical Oceanography, Woods Hole Oceanographic Institution, MS#21,  
360 Woods Hole Road, Woods Hole, MA 02543, USA

<sup>i</sup> Graduate School of Science, Hokkaido University, N10, W8, Sapporo 060-0810, Japan

<sup>j</sup> Naval Research Laboratory, Code 7320, Building 1009, Stennis Space Center, MS 39529, USA

<sup>k</sup> Marine Meteorology Division, Naval Research Laboratory, 7 Grace Hopper Ave, MS2, Monterey, CA 93943-5502, USA

## ARTICLE INFO

### Article history:

Available online 6 July 2008

### Keywords:

Air-sea interaction  
Oceanography  
Meteorology  
Fronts  
Eddies  
Boundary layers  
Kuroshio  
Gulf stream  
Agulhas current

## ABSTRACT

Air–sea interaction at ocean fronts and eddies exhibits positive correlation between sea surface temperature (SST), wind speed, and heat fluxes out of the ocean, indicating that the ocean is forcing the atmosphere. This contrasts with larger scale climate modes where the negative correlations suggest that the atmosphere is driving the system. This paper examines the physical processes that lie behind the interaction of sharp SST gradients and the overlying marine atmospheric boundary layer and deeper atmosphere, using high resolution satellite data, field data and numerical models. The importance of different physical mechanisms of atmospheric response to SST gradients, such as the effect of surface stability variations on momentum transfer, pressure gradients, secondary

\* Corresponding author at: Naval Research Laboratory, Code 7320, Building 1009, Stennis Space Center, MS 39529, USA.  
Tel.: +1 228 688 5974; fax: +1 228 688 4871.

E-mail addresses: [small.ctr.uk@nrlssc.navy.mil](mailto:small.ctr.uk@nrlssc.navy.mil) (R.J. Small), [Simon.deSzeoke@noaa.gov](mailto:Simon.deSzeoke@noaa.gov) (S.P. deSzeoke), [xie@hawaii.edu](mailto:xie@hawaii.edu) (S.P. Xie), [larry.oneill.ctr@nrlmry.navy.mil](mailto:larry.oneill.ctr@nrlmry.navy.mil) (L. O'Neill), [hyodae@atmos.ucla.edu](mailto:hyodae@atmos.ucla.edu) (H. Seo), [qsong@coas.oregonstate.edu](mailto:qsong@coas.oregonstate.edu) (Q. Song), [pcornillon@gso.uri.edu](mailto:pcornillon@gso.uri.edu) (P. Cornillon), [mspall@whoi.edu](mailto:mspall@whoi.edu) (M. Spall), [minobe@mail.sci.hokudai.ac.jp](mailto:minobe@mail.sci.hokudai.ac.jp) (S. Minobe).

circulations and cloud cover will be assessed. The atmospheric response is known to create small-scale wind stress curl and divergence anomalies, and a discussion of the feedback of these features onto the ocean will also be presented. These processes will be compared and contrasted for different regions such as the Equatorial Front in the Eastern Pacific, and oceanic fronts in mid-latitudes such as the Gulf Stream, Kuroshio, and Agulhas Return Current.

© 2008 Elsevier B.V. All rights reserved.

## 1. Introduction

Recent observations of the nature of air–sea interaction over oceanic fronts and eddies have revealed a positive correlation of near-surface wind speed and SST (Liu et al., 2000; Chelton et al., 2001; Hashizume et al., 2001). This is a somewhat surprising result considering that on larger, basin scales, the correlation is often negative (Liu et al., 1994; Mantua et al., 1997; Okumura et al., 2001) which is interpreted as evidence that the atmosphere is driving an ocean response. In the large-scale scenario, intensified winds cool the ocean surface through evaporation, as well as possibly increasing the entrainment of upper-thermocline cool waters into the mixed layer. The opposite type of response over the smaller ocean mesoscale features is suggestive of the ocean forcing the atmosphere, mainly through heat fluxes out of the ocean.

The global nature of air–sea interaction over ocean mesoscale features is illustrated in Figs. 1 and 2 using satellite data from the QuikSCAT scatterometer (launched in 1999), the Tropical Rainfall Measuring Mission (TRMM) Microwave Imager (TMI, launched in 1997), and the AQUA Advanced Scanning Microwave Radiometer for EOS (AMSR-E, launched in 2002). To reveal the scales of interest, filters are applied to the data. Typical ocean eddies have time periods of around 20–30 days at the equator (Tropical Instability Waves, Legeckis, 1977; Lyman et al., 2007) and 100s of days at mid-latitudes, and wavelengths ranging from ~1000 km at the equator (Legeckis, 1977) to 100s of km in mid-latitudes (Stammer, 1997), to 10s of km in high latitudes (e.g. the Iceland–Faroes front, Scott and McDowall, 1990) and coastal zones, approximately following the latitude and stratification dependence of the internal baroclinic Rossby radius of deformation (see, e.g. Killworth et al., 1997; Chelton et al., 1998). Therefore, filtering to remove spatial scales of 1000s of km or more, and temporal scales of a year or more, highlights the ocean mesoscale features and removes longer term modes such as El-Niño Southern Oscillation and Pacific Decadal Variability.

A map of the temporal correlation between high-pass<sup>1</sup> SST and neutral 10 m wind speed from TMI in the region equatorward of latitude 40° (Fig. 1) shows that positive correlation is dominant over most of the domain, reaching up to 0.6 in major frontal zones.<sup>2</sup> Using the shorter record length of AMSR-E, temporal averages of high-pass data<sup>3</sup> over 2 months in boreal summer (Fig. 2) tell a similar story in mid and high latitudes: high-pass filtered wind stress anomaly from QuikSCAT overlies anomalies of SST of the same sign. Here the SST anomalies are associated with the narrow jets and mesoscale eddies of the Kuroshio and its extension (Fig. 2a, see also Nonaka and Xie, 2003), the Gulf Stream and its extension, and the North Atlantic Current (Fig. 2b, see also Chelton et al., 2004), the Brazil–Malvinas confluence in the South Atlantic (Fig. 2c, see also Tokinaga et al., 2005), and the Agulhas Current and Agulhas Return Current (Fig. 2d, see also O'Neill et al., 2003, 2005). The spatial correlation of the anomalous SST and wind stress computed from similar 2-month mean maps range from 0.44 to 0.74 in these major frontal zones (Table 1).

There are several reasons why the atmosphere is affected by ocean fronts and eddies. (i) Firstly, as air is blown across an SST gradient, an air–sea temperature difference and air–sea humidity difference

<sup>1</sup> As the TRMM data is almost a decade long, the data is filtered temporally by removing the first three annual harmonics, and then applying a Fourier analysis and removing variability with time periods of around 40 weeks or more.

<sup>2</sup> Negative correlations of less than –0.2 are only found off Central America in association with gap-wind jets and upwelling (Trasviña et al., 1995), in the Gulf of Aden, and just north of the Mozambique channel.

<sup>3</sup> As the AMSR-E record is short (relative to TRMM), a spatial (Loess) filter has been applied instead, retaining spatial scales of approximately 10° latitude × 30° longitude or less.

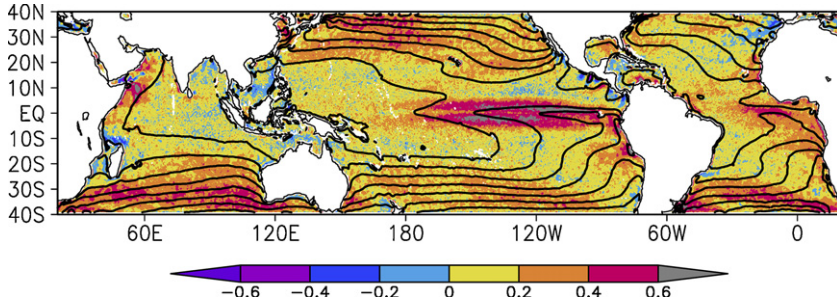


**Fig. 1.** A map of the correlation (color) between SST and neutral 10 m wind speed, both pre-filtered to emphasise mesoscale features. The annual-mean SST ( $^{\circ}\text{C}$ , black contours, interval  $2^{\circ}\text{C}$ , beginning at  $14^{\circ}\text{C}$  and ending at  $30^{\circ}\text{C}$ ) is overlaid. Data from TRMM TMI, 1997–2004. The data was filtered as follows: the first three annual harmonics were first removed, then a Fourier filter has been applied to retain only features of around 40 weeks period or less.

is generated. This leads to changes in near-surface stability and surface stress as well as latent and sensible heat fluxes (Sweet et al., 1981; Businger and Shaw, 1984; Hayes et al., 1989). Changes in stability modify the well-known neutral logarithmic profiles within the surface layer such that the vertical gradients of wind velocity, air potential temperature and humidity are increased in stable

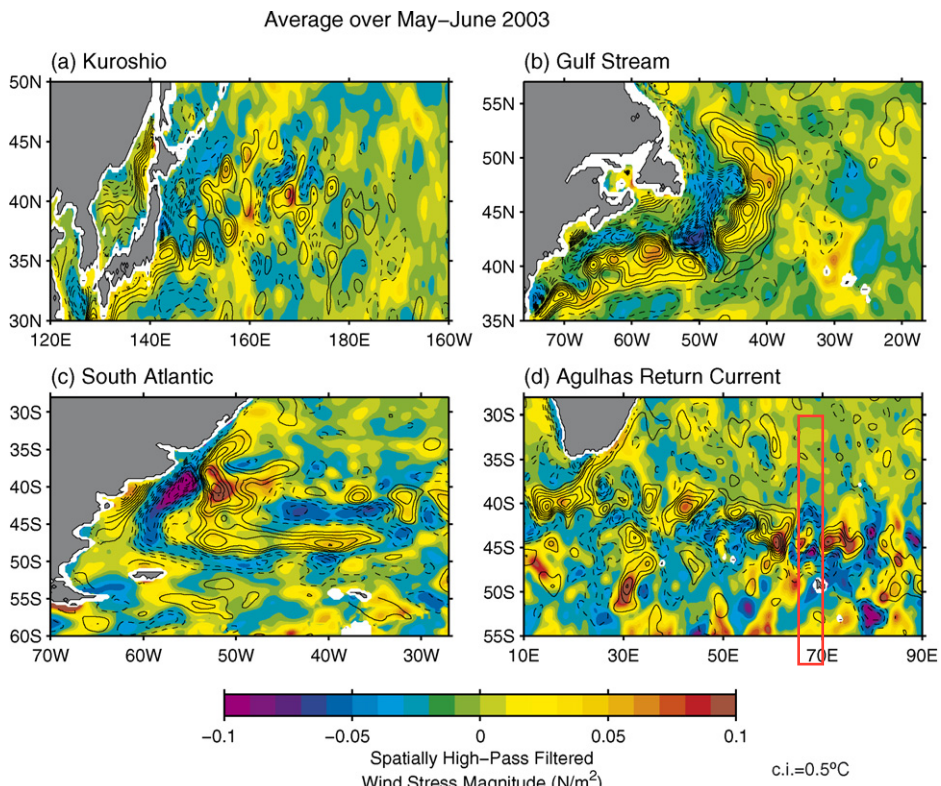


**Fig. 2.** Maps of spatially high-pass filtered 2 months (May–June 2003) average wind stress magnitude ( $\text{N m}^{-2}$ , color) and SST ( $^{\circ}\text{C}$ , contours, interval  $0.5^{\circ}\text{C}$ , zero contour omitted). Data from QuikSCAT scatterometer and AMSR-E. (a) North-west Pacific, Kuroshio region, (b) North-west Atlantic, Gulf Stream and North Atlantic Current region, (c) South-west Atlantic, Brazil–Malvinas confluence, and (d) Southern Indian Ocean, Agulhas Return Current.

**Table 1**

Correlation coefficients computed from the spatial map of high-pass filtered SST and wind stress magnitude shown in Fig. 2

Correlations by region	January–February 2003	July–August 2003
Kuroshio 30° to 55°N, 120°E to 160°W	0.440	0.438
Gulf Stream 35° to 60°N, 80°W to 15°W	0.569	0.568
South Atlantic 30° to 60°S, 70°W to 25°W	0.645	0.742
A�ulhas 30° to 60°S, 0° to 100°E	0.631	0.649
Global	0.39	0.42

The coefficients are given for the four defined regions and for a near-global domain (from 70°S to 70°N), and for boreal winter and summer 2003.

conditions or decreased in unstable conditions (see, e.g. [Stull, 1988](#)). (ii) The turbulent fluctuations of heat, moisture and momentum may be transported deeper into the boundary layer by large eddies, one result being a transfer of momentum from the upper boundary layer towards the surface ([Hayes et al., 1989; Wallace et al., 1989](#)). This will also lead to changes in the height of the boundary layer. (iii) As the air temperature and moisture start to respond to the surface fluxes, the atmospheric pressure also changes ([Lindzen and Nigam, 1987](#)). This leads to a spatial pressure gradient which can drive secondary circulations ([Wai and Stage, 1989](#)). (iv) The surface currents of ocean fronts or eddies will impact the relative motion of the air and ocean, acting to change the surface stress, thus affecting the atmosphere as well as feeding back onto the ocean ([Kelly et al., 2001; Cornillon and Park, 2001](#)).

There has been much debate on the relative contributions of the momentum mixing and the pressure gradient effects in changing the wind profile ([Chelton et al., 2004](#)). In the 1980s observational papers originally attribute the positive correlation to the effects of surface stability on the vertical transfer of momentum in the boundary layer ([Sweet et al., 1981; Wallace et al., 1989; Hayes et al., 1989](#)), but a series of modeling papers studying cold-air outbreaks over the Gulf Stream showed the importance of secondary circulations and pressure-driven flows in the interaction ([Huang and Raman, 1988; Wai and Stage, 1989; Warner et al., 1990](#)). Since the 1990s the large increase in observations afforded by scatterometers (with nearly global coverage of wind stress over the ocean every day, [Liu et al., 2000](#)), passive microwave instruments (which detect the SST through clouds, [Wentz et al., 2000](#)) and infrared radiometers (which have a high spatial resolution) led to the finding that the positive correlation is almost ubiquitous ([White and Annis, 2003; Small et al., 2005a](#), see [Figs. 1 and 2](#)), but has not yet resolved the debate over the mechanism. However, the synthesis of high resolution numerical modeling with the satellite data and intensive *in situ* campaigns has lead to a deeper understanding of the problem. This paper summarizes the findings of these new results in the context of the earlier work.

The atmospheric response problem is not purely academic: [Chelton et al. \(2004\)](#) have shown that associated with this process are small-scale wind stress curl and divergence features that may significantly affect ocean circulation. These findings suggest that the full air–sea coupled problem needs to be understood, rather than just one component, in order to explain the observations and improve model forecasts. Further, the changes in sensible and latent heat flux which occur over the small scales of the oceanic fronts are likely to be significantly underestimated by reanalysis models with resolutions of 1° or more, as shown by [Rouault et al. \(2003\)](#). This in turn may lead to an underestimation of the modification of extra-tropical storms by the surface fluxes ([Kuo et al., 1991; Holt and Raman, 1992](#)).

The air–sea interaction over ocean fronts has been the subject of two recent review papers. [Xie \(2004\)](#) emphasized how the response over cool waters (less than about 27 °C) is markedly different to the response over warm waters, where, as illustrated by El-Niño, the ocean SST and heat content modulates the amount of deep convection. In contrast, over the cooler seas the response may be more confined to the boundary layer, where the latent and sensible turbulent flux changes at a front alter the boundary layer temperature, and the wind profile adjusts to the changes in mixing and the induced hydrostatic pressure gradients. [Chelton et al. \(2004\)](#) focused on the wind stress curl and divergence response to fronts and eddies, and showed an approximately linear response of the curl to the crosswind SST gradient, as well as the divergence to the along wind SST gradient, over all the ocean basins. Long and distinct curl signatures are seen at fronts such as the Gulf

Stream, Kuroshio, Agulhas current and the Equatorial Front, as well as over their associated eddy features. These anomalies of wind stress curl may have a significant impact on the ocean, as discussed in Section 4.

The aim of this paper is to update these findings and focus on two aspects of the air-sea interaction which were only discussed in brief in these previous reviews: the mechanism of atmospheric wind adjustment, and the feedback onto the ocean. Firstly, in Section 2, observations of air-sea interaction will be described for three case studies representing equatorial and higher latitude regimes, and northern and southern hemispheres: the Equatorial Front in the Eastern Pacific, the Gulf Stream, and the Agulhas Current/Retroflection region. Then the physical process of the atmospheric boundary layer response to SST changes will be described in Section 3, using established numerical results to complement the observational findings. (The main findings of Sections 2 and 3 are summarized in Sections 2.4 and 3.3, respectively, which the reader may wish to read first.) In Section 4 the potential feedback from the atmosphere to the ocean will be discussed, as well as some numerical simulations of the fully coupled air-sea interaction process. Section 5 presents a discussion, and the concluding Section 6 includes a summary and identifies how the field has progressed, as well as current gaps in knowledge.

## 2. Atmospheric wind response to fronts and eddies: case studies from observations

The atmospheric response to SST distributions has been an area of long and rich study. Indeed [Halley \(1686\)](#) described the trade winds as the response to heating the air over the warmer ocean surface. Having lower density, the heated air rises, and is replaced by wind flowing from higher latitudes. This air gains an easterly component to conserve angular momentum ([Hadley, 1735](#)). In the late 20th Century the debate focused on how the atmospheric circulation responded to SST anomalies and gradients. [Gill \(1980\)](#) proposed a model of the tropical atmospheric circulation response to heating in the mid-troposphere. In this scenario convection anomalies drive low-level wind anomalies and convergence. Although this model made no explicit reference to SST, subsequent papers added a simple dependence of heating on SST ([Gill and Rasmusson, 1983](#); [Philander et al., 1984](#); [Hirst, 1986](#)). More sophisticated models then included the feedback effect of low-level moisture flux convergence onto surface flux and hence heat anomaly (e.g. [Zebiak, 1986](#)). An alternate model by [Lindzen and Nigam \(1987\)](#) related the circulation directly to the SST by hydrostatic pressure gradients induced in the marine atmospheric boundary layer (MABL). In their model surface winds near the equator (where the Coriolis parameter  $f$  is small) would consequently flow down the pressure gradient from cool SST to warm SST. The anomalous MABL wind field gradients then cause convergence of water vapor, leading to deep convection. Although it has been shown that the Gill model (as modified by [Zebiak, 1986](#) to include SST) is mathematically similar to the Lindzen–Nigam model ([Neelin, 1989](#); [Battisti et al., 1999](#)), the physical basis behind these models is different.

These models typically apply to large, basin-scale SST anomalies, to which the atmosphere has sufficiently large time to adjust, and are also appropriate for the tropics where the SST is high enough to initiate deep convection, such as in the warm pool regions. The processes which occur over mesoscale ocean SST anomalies, particular those occurring outside the warm pool, may be different than those that occur at basin scale.

Due to the different densities of water and of air, mesoscale features such as fronts and eddies tend to be much smaller in the ocean (on the scale of the first baroclinic Rossby radius, [Chelton et al., 1998](#)) than in the atmosphere. For example high resolution ship surveys of the Equatorial Front in the eastern Pacific have determined that the temperature change occurs over less than 20 km ([Yoder et al., 1994](#)), and close to Bermuda a 2 °C change occurred over 100 m ([Khalsa and Greenhut, 1989](#)), and ocean eddies typically have diameters on the order of 100 km in contrast to atmospheric pressure systems (1000 km). As a consequence, when the atmospheric wind blows across ocean fronts, it leads to rapid localised changes in the MABL.

One of the first intensive studies of air-sea interaction over fronts and eddies was the Joint Air-Sea Interaction (JASIN) experiment in the North Rockall Trough (59°N, 13°W) in the Atlantic in summer of

1978.<sup>4</sup> Businger and Shaw (1984) presented an analysis of the effect of ocean eddies on the atmospheric boundary layer using JASIN data and the Brown and Liu (1982) MABL model. During late summer of 1978, a cold atmospheric front passed a well instrumented array of moorings. The array measured a rapid increase in latent and sensible heat fluxes and wind stress as the cold-air flowed from cool water towards an area of warm SST, in agreement with the predictions of the model. Businger and Shaw explained this with a conceptual model of MABL response to a warm eddy:

- (a) The boundary layer height increases in response to the larger turbulent heat fluxes, possibly leading to thicker stratocumulus where present.
- (b) A modest 'heat-island effect' or 'land breeze' occurs with winds flowing into the eddy.
- (c) The increased drag over the warmer water slows the wind over the eddy. Thus, there is wind convergence on the upwind side and divergence on the downwind side. [Author's note: this is the only part of the Businger and Shaw paper that appears to be directly refuted by later observations and models. In the results described below, it will be shown that although the drag increases over a warm eddy, the wind speed also increases. This leads to wind divergence on the upwind side and convergence on the downwind side.]
- (d) The stress over the warm eddy increases as a result of the higher drag. For westerly winds this induces positive wind stress curl on the northern edge and negative curl on the southern edge.

These early findings (based on limited flight passes across an eddy) from JASIN and measurements across the Gulf Stream front by Sweet et al. (1981) raised interest in performing more detailed analysis of the processes involved. In the following decades further intensive experiments such as the Frontal Air–Sea Interaction Experiment (FASINEX, Friehe et al., 1991), the Genesis of Atlantic Lows Experiment (GALE, Dirks et al., 1988), the Structure des Exchanges Mer–Atmosphère, Propriétés des Hétérogénéités Océaniques experiment (SEMAPHORE, Eymard, 1998), and East Pacific Investigation of Climate Processes (EPIC, Raymond et al., 2004), together with enhanced instrumentation on moorings such as the Tropical–Atmosphere–Ocean (TAO) array, high resolution satellite data, and numerical models have been used to test these hypotheses. As will be seen below, some have stood the test of time whilst others have been refuted or modified.

In this section, firstly three regions are discussed in detail to describe, illustrate, and compare proposed mechanisms of MABL response to underlying SST gradients. The focus is on how the wind profile is adjusted, as this is a question of much debate: but findings on the thermodynamic structure of the response are also discussed for completeness. Then, in Section 2.4, a summary of the observed changes in MABL (MABL) over ocean fronts is given.

## 2.1. Equatorial front and tropical instability waves

In the eastern portions of the Pacific and Atlantic Oceans, equatorial upwelling driven by the Ekman divergence of trade winds creates a cold tongue of water for most of the year. These tongues are bordered by a sharp SST front to the north (referred to as the Equatorial Front) and a somewhat weaker front to the south (e.g. Fig. 3a, showing the Equatorial Pacific). Meanders along the fronts have become known as Legeckis eddies or Tropical Instability Waves (TIWs: Düing et al., 1975; Legeckis, 1977), and are observed to grow in the east and propagate westwards (see Lyman et al., 2007, for a review). The unusual property of these fronts of being on or very close to the equator allow an examination of the air–sea interaction processes in the absence of strong effects of rotation.

In their seminal study of the surface winds over the Pacific cold tongue, Wallace et al. (1989) showed from monthly mean Comprehensive Ocean–Atmosphere Data Set (COADS) wind and SST fields that the SST frontal region was not the region of the strongest surface wind speed predicted by the

<sup>4</sup> See, e.g. 'Results of the Royal Society Joint Air–Sea Interaction project (JASIN)', Proceedings of a Royal Society discussion meeting held on 2 and 3 June 1982, ed. H. Charnock and R.T. Pollard, pub Royal Society London 1983, also in Philos. Trans. R. Soc. Lon. A, 308, 221–429.

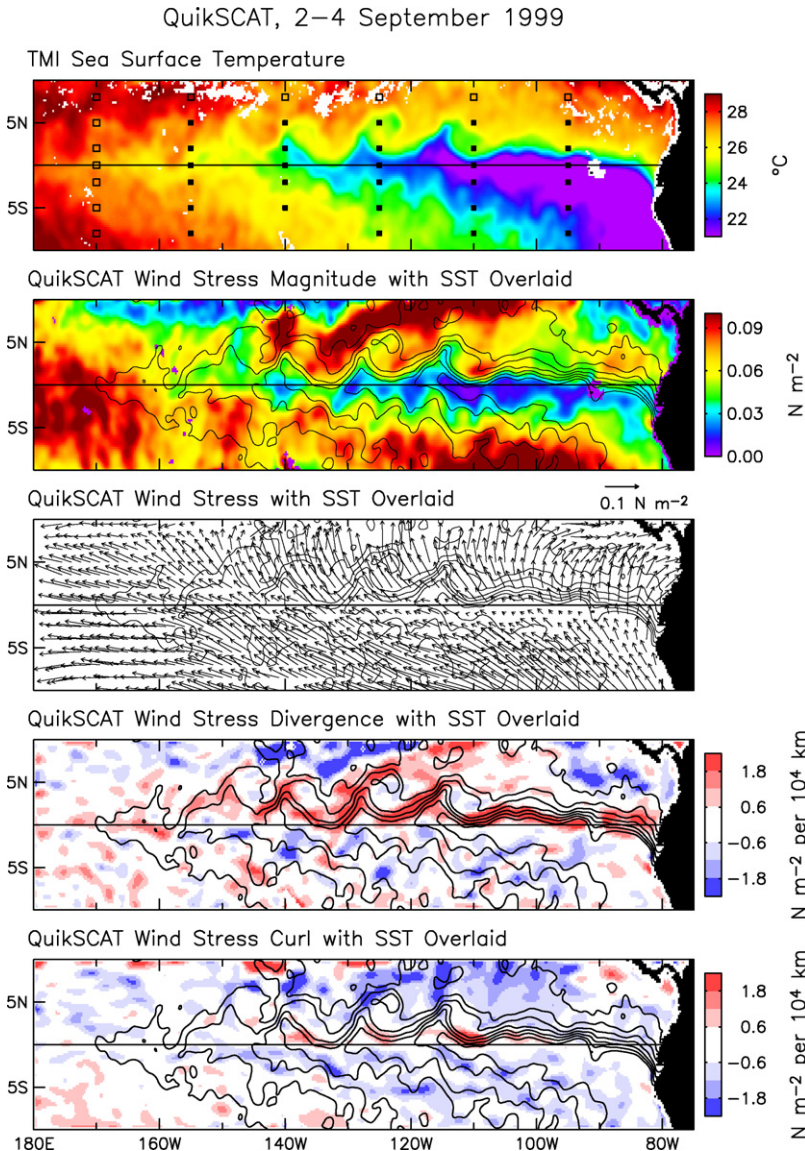


**Fig. 3.** Three-day average maps over the period 2–4 September 1999 showing Tropical Instability Waves. (a) Sea surface temperature with TAO mooring locations shown as squares; (b) wind stress magnitude; (c) wind stress; (d) wind stress divergence; and (e) wind stress curl. The contours overlaid in (b)–(e) correspond to isotherms at intervals of 1 °C between 21 and 27 °C. From Chelton et al. (2001). Reproduced by permission of the American Meteorological Society.

Lindzen–Nigam model, but of the strongest surface wind divergence. Wallace et al. (1989) formulated a mechanism to explain this discrepancy. They hypothesized that vertical transfer of momentum by mixing was adjusting the surface winds. In this explanation, over the stable conditions of the cold tongue, an upper level south-easterly wind jet is well-separated from weaker surface winds. The near-surface air becomes more unstable when passing across the front towards warmer water, leading to enhanced mixing in the boundary layer, and momentum from the upper easterly jet is brought down to the surface, accelerating the surface wind.

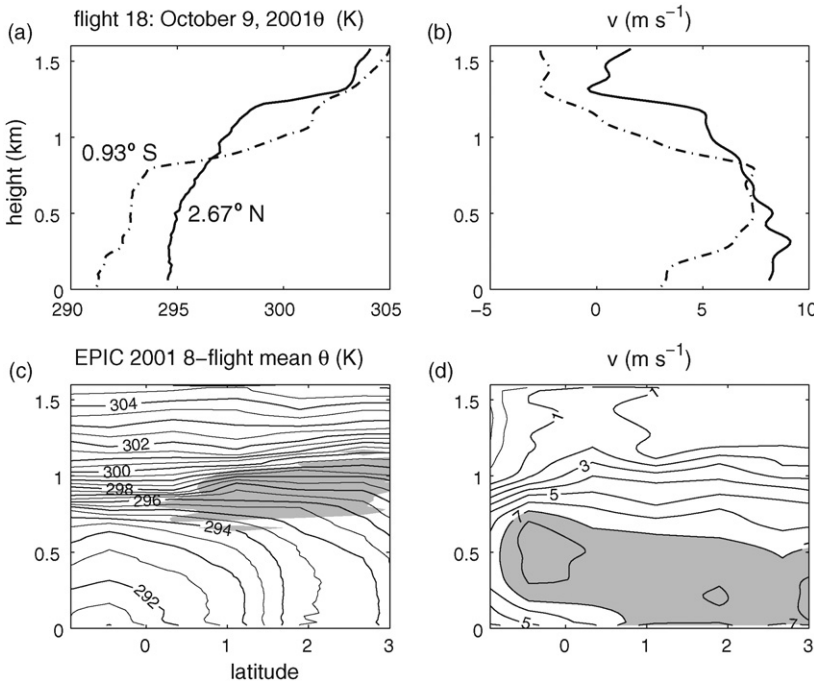


**Fig. 4.** EPIC 2001 observations of the MABL across the Equatorial Front at 95°W. Potential temperature (a) and meridional velocity (b) from representative dropwindsondes in the cold tongue (dot-dash) and north of the front (solid). (c and d) Cross-sections, respectively, of potential temperature and meridional velocity, composited from in situ data from 8 flights by the NCAR C-130 aircraft. The gray shading in (c) encloses the region where cloud liquid water is greater than  $0.1 \text{ g kg}^{-1}$ . Adapted from deSzeoke et al. (2005). Reproduced by permission of the American Meteorological Society.

In situ data from a single ship survey of the Equatorial Front at 125°W in September 1998 (Anderson, 2001) confirmed the analysis of COADS data. In particular, an increase of 4°C across 2.5° latitude was found to coincide with an increase of meridional wind from 2 to 5 m s<sup>-1</sup>, and a change of sea-air temperature difference from 0.3 to 1.2 °C. Meanwhile sea level pressure was reported to drop 2 hPa from the south side of the cold tongue to the far side of the north wall at 5°N.

The coupled air-sea system in the eastern tropical Pacific was the subject of more detailed investigation during the EPIC field experiment (Raymond et al., 2004). The specific aims of EPIC included the investigation of convection in the Intertropical Convergence Zone (ITCZ), the dynamics of cross-equatorial flow, and the maintenance of the southeast Pacific tropical stratocumulus deck. As well as long period (3–4 years) enhanced monitoring at TAO moorings and in the south-east Pacific, an intensive aircraft and ship campaign took place in September–October 2001.

As part of EPIC, eight aircraft missions measuring winds, temperature, humidity, turbulence, and turbulent fluxes were flown through the MABL along 95°W to investigate the nature of the cross-equatorial flow. Turbulent fluxes of heat and momentum were calculated from aircraft observations at 30 m (deSzeoke et al., 2005), which showed that the latent and sensible heat fluxes were nearly zero over the cold tongue, and 180 and 30 W m<sup>-2</sup>, respectively, at 2°N. These large heat fluxes on the north side of the cold tongue were a source of buoyancy and mixing in the lower boundary layer, and contributed to MABL clouds and entrainment at the MABL top. Individual soundings (Fig. 4a) and the composited 95°W vertical cross-section (Fig. 4c) show that the atmospheric mixed layer increases with height as the front is crossed, as well as the boundary layer and inversion layer height. A wind jet at 500 m was observed over the equator above low surface wind speeds, whilst north of the cold tongue the mid-level jet appeared to descend towards the surface, with maximum near-surface winds at around 3–4°N (Fig. 4b and d). McGauley et al. (2004) found the strongest northward pressure gradient

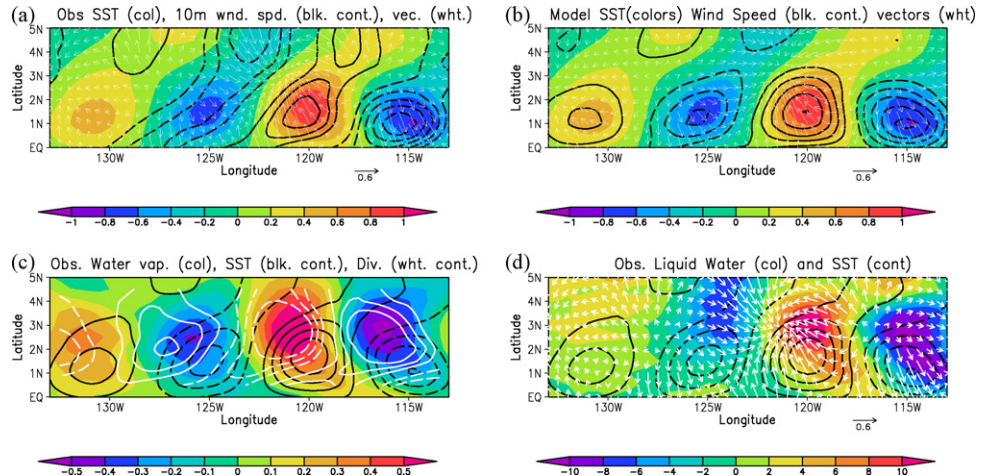


**Fig. 5.** Composite regression onto SST at a center point of 120°W, 2°N. (a) Observed SST (color) and wind velocity ( $\text{m s}^{-1} \text{K}^{-1}$ , see scale arrow) and wind speed ( $\text{m s}^{-1}$ , contours,  $0.1 \text{ m s}^{-1} \text{K}^{-1}$  interval), (b) Regional Atmospheric Model wind velocity ( $\text{m s}^{-1} \text{K}^{-1}$ , see scale arrow) and wind speed ( $\text{m s}^{-1} \text{K}^{-1}$ , contours,  $0.1 \text{ m s}^{-1} \text{K}^{-1}$  interval) forced by observed SST (color) at the surface, (c) column integrated water vapor (color,  $\text{mm K}^{-1}$ ), SST (black contoured at 0.1 intervals) and wind convergence ( $\text{s}^{-1} \text{K}^{-1}$ , white contours, contoured for  $\pm 1, 2, 3 \times 10^{-6} \text{ s}^{-1} \text{K}^{-1}$ ), (d) column integrated cloud liquid water (color,  $10^{-3} \text{ mm K}^{-1}$ ) and SST (contoured at 0.1 intervals). Adapted from Small et al. (2003). Reproduced by permission of the American Meteorological Society.

force at 2–3°N, due to the warmer boundary layer temperature on the north side of the SST front. Meridional surface stress also increased on the north side of the front, from 0.02 Pa at 0.8°S to 0.08 Pa at 0.6°N according to bulk measurements from the aircraft (deSzeoek et al., 2005).

The atmospheric response to TIWs was first observed by Hayes et al. (1989) from early TAO measurements. By computing the meridional difference in wind velocity (e.g. from the equator to 2°N), they were able to isolate TIW-induced fluctuations from large-scale, coherent wind structures. Hayes et al. found that there was a positive correlation between SST and southeasterly wind anomalies, with enhanced wind over the warm phase of TIWs. They attributed this to the momentum mixing mechanism of Wallace et al. (1989). Xie et al. (1998) utilised the broader coverage allowed by the European Remote Sensing (ERS) satellite scatterometer data and Advanced Very High Resolution Radiometer (AVHRR) SST data to produce spatial maps of TIWs and associated wind fields. By applying a high-pass spatial filter in the zonal direction they confirmed Hayes et al.'s (1989) findings obtained from the more limited in situ data. These results were refined by the much better temporal sampling of the eddies obtained by the QuikSCAT scatterometer<sup>5</sup> (Fig. 3b and c) as shown by Liu et al. (2000), Chelton et al. (2001), and Hashizume et al. (2001). The relationship between SST and wind stress fields is seen more clearly in a spatial map of the one-point regressions of high-pass filtered SST and wind vectors (Fig. 5a, modified from Hashizume et al., 2001; Small et al., 2003). The amount of water vapor in the atmospheric column is enhanced over the TIW-induced wind convergence (Fig. 5c), associated with increased evaporation and moisture convergence. Cloud liquid water is enhanced over and downstream of the warm SST (Fig. 5d). Ship-board soundings by Hashizume et al. (2002) show that the MABL deepens over the warm phase of TIWs, favoring formation of stratocumulus clouds, as observed from satellite by Deser et al. (1993).

From measurements at TAO moorings, Thum et al. (2002) showed that individual TIWs were associated with sensible and latent heat fluxes per °C of SST anomaly of around  $4 \text{ W m}^{-2}$  and  $33 \text{ W m}^{-2}$  (almost in phase with SST), respectively. These significant fluxes arise because the atmosphere is slow to respond to sharp SST gradients, leading to an air-sea temperature difference (Xie, 2004). Cronin et al.

<sup>5</sup> The ERS satellites cover 41% of the global ocean daily, compared with 93% for QuikSCAT.

(2003) determined from enhanced TAO observations that the surface pressure responded by around 0.11 hPa per  $^{\circ}\text{C}$ , with the negative of the pressure ( $-p$ ) leading the SST anomaly by around 4 days. As expected by hydrostatics, negative pressure anomalies were also found to be close in phase to air temperature. Advection by the mean easterlies shifted the air temperature and resultant hydrostatic pressure response downstream of the SST anomaly.

Chelton et al. (2001) investigated TIWs and found that positive wind stress curl was generated when the wind blew along the SST isotherms of the northern TIW front, due to the shear between the higher speeds to the right and lower speeds to the left of the air parcel (Fig. 3e). This led to an observed linear relationship between wind stress curl and crosswind component of SST gradient. Likewise wind stress divergence occurred as the air flows across the front (Fig. 3d), and was found to be linearly related to the along wind component of SST gradient.

Most studies of equatorial fronts and TIWs have focused on the Pacific Ocean, but it should be mentioned that the Atlantic Ocean also has these features, although the cold tongue season in the Atlantic is much shorter than in the Pacific, and is linked to continental influences such as the African summer monsoon (Mitchell and Wallace, 1992). The properties of Atlantic TIWs, and their relationship to the mean state and the MABL, have been studied by, e.g. Seo et al. (2006, 2007b), and Wu and Bowman (2007).

## 2.2. Gulf Stream and north Atlantic

In contrast to the Equatorial Front, which lies in an almost steady trade wind regime, western boundary currents (WBCs) and their associated SST gradients are often located in regions of variable winds, such as the mid-latitude storm tracks. Further, unlike the flow over the Equatorial front, flow over the WBCs will be influenced by the Earth's rotation. Therefore, for comparative reasons it is useful to assess how the atmosphere responds to WBCs such as the Gulf Stream (discussed here), the Agulhas current (Section 2.3) and the Kuroshio (see Nonaka and Xie, 2003; White and Annis, 2003), together with their more zonally aligned extensions.

The Gulf Stream is a strong poleward warm current in the western Atlantic with a large transfer of heat from the ocean to the atmosphere (see, e.g. Stommel, 1966; Tomczak and Godfrey, 1994). During the late winter and early spring, the temperature is about  $10^{\circ}\text{C}$  warmer than the adjacent Continental Slope Water to the north (Sweet et al., 1981). The associated large temperature gradient at the edge of the current produces significant atmospheric changes, which have often been noted by observers crossing the northern edge of the Gulf Stream. The Gulf Stream system can be considered in many ways to be an ideal experimental laboratory for observing frontal air-sea interaction processes.

Several in situ experiments have studied the atmospheric response to the Gulf Stream and eddies. Sweet et al. (1981) reported changes in sea state, boundary layer winds and temperature across the front. The sea was rougher over the warm Gulf Stream, indicating a statically unstable interface. (A similar example of sea state change is illustrated in Fig. 6a.) In one flight, wind speed was greater (18–20 kt) and mixed layer deeper (914 m) over the Gulf Stream, compared to 8–10 kt and 600 m, respectively, over the slope water.

Analysis of the sea state variations seen in photographs such as Fig. 6a has been extended by various authors using spaceborne Synthetic Aperture Radar (SAR), which detects the centimetre to metre scale waves on the sea surface. Weissman et al. (1980) produced the first analysis of SAR imagery of the Gulf Stream and how it depended on the wind speed and SST. Sikora et al. (1995) noted distinct surface roughness patterns either side of the Gulf Stream North Wall in one particular image (reproduced in Fig. 6b). Ship-board measurements of the air-sea temperature difference (Fig. 6c) showed that the air-sea interface changed from stable to unstable across the Gulf Stream North Wall. On the east (warm) side, in unstable surface conditions, a 'mottled' surface pattern was taken to represent cellular convection, whereas over the cool SST to the west, a 'marbled' pattern with generally low backscatter and some curvilinear dark features was taken to represent low wind speed, stable conditions interspersed by oceanic frontal regions organizing surfactants into the linear features. Beal et al. (1997) compiled a detailed intercomparison of SAR and AVHRR images which showed that the character of the sea surface change across the Gulf Stream North Wall also depended on background wind direction. They interpreted the data in terms of a combined MABL model (based on Brown, 1982) and

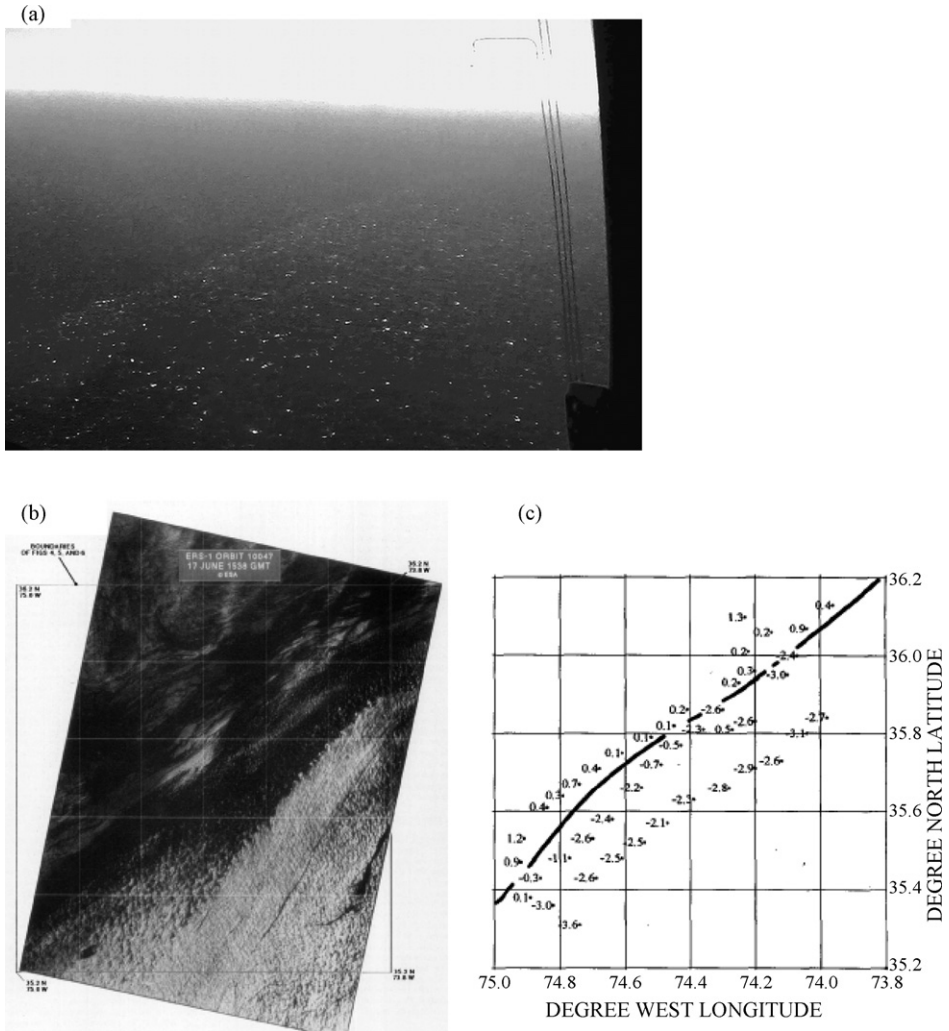


**Fig. 6.** (a) Photograph taken from the National Oceanic and Atmospheric Administration (NOAA) P-3 aircraft looking towards the northeast across the north wall of the Gulf Stream. The winds were blowing from the northeast at the time of the photograph. The seas were calm over the colder waters to the northwest of the Gulf Stream (upper left) and white caps covered the warmer water to the southeast (Courtesy of P. Chang and D. Chelton). From Chelton et al. (2006). Reproduced by permission of American Meteorological Society. (b) European remote sensing satellite ERS-1 synthetic aperture radar image of 17 June 1993 showing convective cells over Gulf Stream water (bottom right): smooth waters over cool shelf water (top left), and (c) corresponding map showing the position of the Gulf Stream North Wall (solid line) and spot values of 10 m air temperature minus SST from near-coincident ship measurements. Note that the gridded domain in (c) matches that shown over the image in (b), namely from 75°W to 73.8°W, and 35.2°N to 36.2°N, with a grid spacing of 0.2°. From Sikora et al. (1995). Reproduced by permission of the American Meteorological Society.

backscatter model using surface stability conditions measured from ship, which confirmed that step changes in backscatter were due to changes in stability. However, they also noted that 'sea-breeze' effects, due to pressure gradients set up by thermal contrast across the front, were important.

It has long been known that besides their direct modification of the MABL, ocean fronts can influence synoptic storms. For instance, storm tracks measured in terms of cyclone frequency (Colucci, 1976) or synoptic variability of surface stress (K. Kelly, personal communication) are located close to the

Gulf Stream system. Indeed the rapid deepening of storms known as "Bombs" (defined as an extra-tropical surface cyclone with a surface pressure that falls on the average at least  $1 \text{ hPa h}^{-1}$  for 24 h) has been observed to occur over the north flank of the Gulf Stream and Kuroshio (Sanders and Gyakum, 1980; Sanders, 1986; Cione et al., 1993). Some of these intense synoptic or mesoscale storms can have unusual warm cores, related to a 'bent-back' warm front, more akin to tropical cyclones than typical extra-tropical lows (Neiman and Shapiro, 1993; Businger et al., 2005).

The response of synoptic storms to the Gulf Stream was investigated as part of GALE (Dirks et al., 1988). The main focus of this large, multi-institution experiment was to study severe storms which typically develop off the East Coast of USA in winter and track northwards to later affect the north-eastern states. Cyclogenesis was found to be affected by offshore latent heat release and the appearance of coastal fronts. Air-sea temperature differences of up to  $24^\circ\text{C}$  were found to be associated with surface turbulent heat fluxes up to  $1200 \text{ W m}^{-2}$  occurring in individual storms (Doyle and Warner, 1990). Coastal atmospheric fronts were found to be typically aligned with either the Gulf Stream oceanic front or shelf fronts. Holt and Raman (1992) noted that the coastal front was a relatively shallow atmospheric front (less than 500 m deep) with higher clouds on the warm side of the front than over the cold side, where clouds at 200 m lay above the internal boundary layer. Waves can develop along these coastal fronts and Doyle and Warner (1990) and Holt and Raman (1992) suggest that they can influence cyclogenesis, by providing a source of low-level positive vorticity and moisture. In ideal conditions the combination of a baroclinic zone at the surface (surface temperature gradient) and a positive vorticity anomaly (or short wave trough) aloft is ideal for amplifying synoptic storms, as discussed in the framework of baroclinic instability theory by Hoskins et al. (1985) and summarized in Holton (2004).

Recently, observations of Gulf Stream sea surface properties have been greatly enhanced due to the advent of microwave imaging satellite radiometers and satellite scatterometers such as QuikSCAT, ERS and Adeos II. This has enabled the fine structure of the atmospheric response to the Gulf Stream to be detected, as shown by Chelton et al. (2004) and Xie (2004). In particular it can be seen that there is a close co-location between extrema in 3-year mean SST seen from AMSR-E and extrema in the mean scalar 10 m neutral wind speed measured by QuikSCAT (Fig. 7a), with the highest speeds (equivalently, largest stress magnitude) over warmer SST. The Gulf Stream also causes a signature in wind stress divergence and curl, the former being mostly due to acceleration of the winds which flow across the Gulf Stream in the mean (particularly north east of Cape Hatteras, Chelton et al., 2004). The wind curl signature is partly due to the atmospheric response and partly due to the ocean currents, which may increase/decrease the stress when wind flows against/with the current (Kelly et al., 2001; Chelton et al., 2004), as discussed in Section 4.2.

The fact that the Gulf Stream has an effect on clouds has been recognized for many years (e.g. Carson, 1950). Young and Sikora (2003) performed a detailed analysis of the atmospheric mesoscale cloud formations which occurred when cold-air flowing from the continent in winter behind synoptic storms is advected across the warm Gulf Stream. Many beautiful visible and infrared images showed mesoscale cloud bands forming on the upstream edge of the Gulf Stream north wall and trailing downstream (Young and Sikora, 2003). Sublette and Young (1996) documented a summer situation when background synoptic variability was weak and the SST gradients lead to a convergence zone, and boundary layer cloud, over the Gulf Stream. A map of the annual mean cloud liquid water in the North Atlantic from AMSR-E (Fig. 7b) shows a band of high liquid water content closely following the warm waters of the Gulf Stream and North Atlantic Current. Recent satellite observations of albedo from space also show a high correlation with underlying SST (Dudley Chelton, personal communication).

In addition to the Gulf Stream current, the response over the eddies shed by the Gulf Stream has also been analyzed. Recent studies by Cornillon and Park (2001), Park and Cornillon (2002), and Park et al. (2006) have demonstrated how ocean currents and changes in MABL stability associated with Gulf Stream rings affect the surface wind stress observed by scatterometers. In their study, the relationship between satellite-derived 10 m equivalent wind,  $U_{10}^N$ , and  $T_{\text{sea}} - T_{\text{air}}$  (where  $T_{\text{sea}}$  denotes SST and  $T_{\text{air}}$  is the near-surface air temperature) in the vicinity of Gulf Stream rings was examined, using the sea surface temperature differences between water in the ring and water that surrounds it as a proxy for  $T_{\text{sea}} - T_{\text{air}}$ . (This assumes that the air is equilibrated to the ocean surface temperature outside

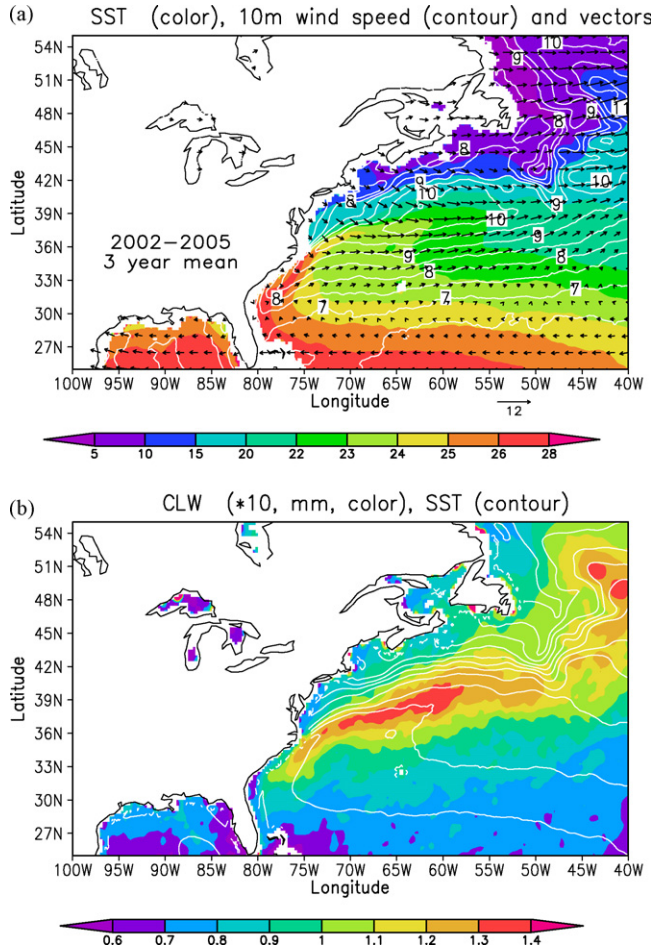


**Fig. 7.** (a) North-west Atlantic annual mean SST (color,  $^{\circ}\text{C}$ , note the non-linear scale) and mean neutral 10 m wind speed ( $0.5 \text{ m s}^{-1}$  contour interval), and vectors (see scale at bottom right), (b) column integrated cloud liquid water ( $10^{-1} \text{ mm}$ , color) and SST (contours at  $2^{\circ}\text{C}$  intervals, odd integers). A 3-year mean from June 2002 to June 2005 has been used, with SST and cloud liquid water from AMSR-E and 10 m winds from QuikSCAT.

the eddy, but does not have time to adjust its temperature when passing over the eddy. This is likely to overestimate the air-sea temperature difference as in reality the air will partially adjust to the eddy SST.) Park et al. (2006) found that near-surface wind speeds increase by about 10% over warm core rings and reduce by around 15% over cold core rings (Fig. 8). Over warm core rings the strongest wind speeds are found over the core of the ring (Fig. 8a and b), consistent with boundary layer modification. Over cold core rings, the lowest speeds are found over and to the right of the core where the ocean current has a component in the same direction as the wind (Fig. 8c and d), so that the relative velocity is less than the wind speed: this suggests that the ocean currents are also modifying the measured stress. Over warm core rings there is strong divergence (convergence) on the upwind (downwind) side, while curl is strongly negative on the south edge of the ring boundary and positive on the north edge. The opposite patterns are seen over cold core rings. An important effect of the enhanced convergence on the downwind side of warm core rings is seen in cloudiness fraction data from SST images, which reveals substantially enhanced cloud probabilities on the downwind side (Park et al., 2006).

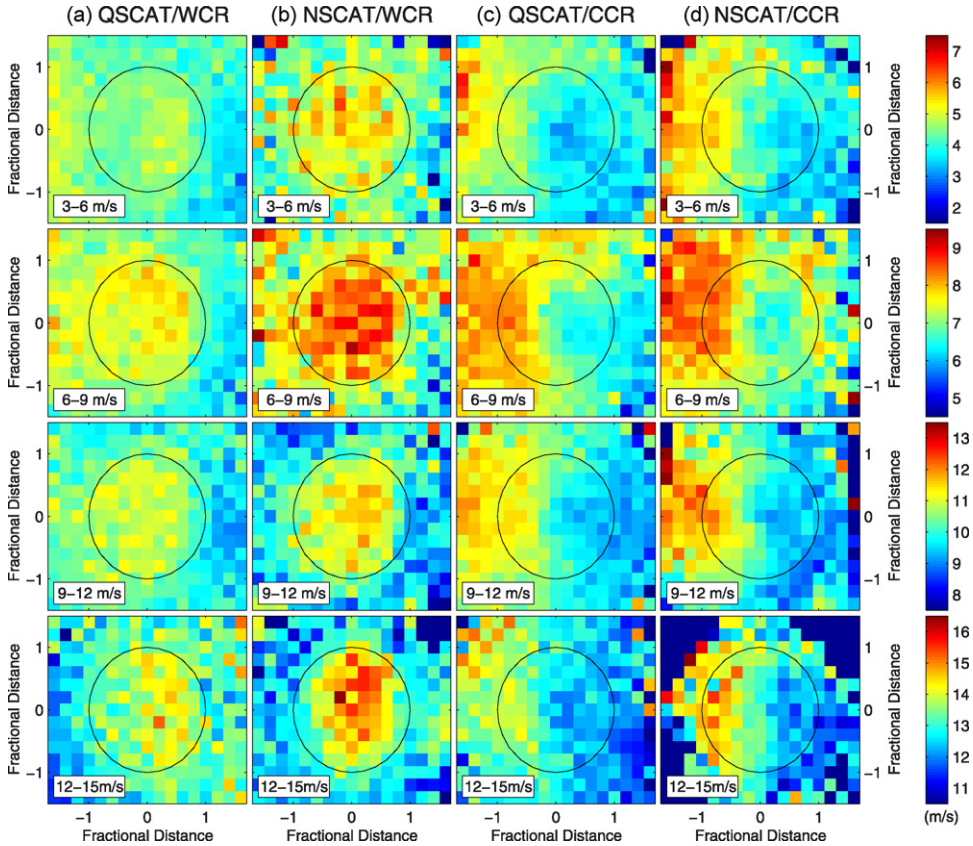


**Fig. 8.** Gulf Stream rings. Component of scatterometer winds (color,  $\text{m s}^{-1}$ , see color-scale at right) along the mean wind direction, in ring-centric coordinates rotated such that the mean wind is towards the top of the figure. Each row denotes a different mean wind speed (as labelled). (a) Warm core rings from QSCAT, (b) warm core rings from NSCAT, (c) cold core rings from QSCAT, (d) cold core rings from NSCAT. Fractional distance denotes the distance from the eddy center scaled by the eddy radius. From Park et al. (2006). Copyright American Geophysical Union (2006) and reproduced by their permission.

### 2.3. Agulhas current/retroflexion

Within 70 km of the coast of South Africa, the Agulhas Current flows southwestward from the Indian Ocean before separating from the coast and turning abruptly along the southern tip of South Africa at the Agulhas Retroflexion and continuing eastward as the Agulhas Return Current (Boebel et al., 2003a).

Several cyclonic and anti-cyclonic “Agulhas rings” and eddies are shed from the Agulhas Retroflexion every year, each having a large surface expression that can persist several months as they propagate into the south Atlantic basin (Boebel et al., 2003b). Bathymetric-induced meanders along the Agulhas Return Current create alternating series of positive and negative SST perturbations in the SST front (Lutjeharms and van Ballegooyen, 1984) that are generally quasi-stationary (Pazan and Niiler, 2004). These features produce a rich array of small spatial scale ( $\sim 100$ –1000 km) SST perturbations, which are illustrated in the 2 months mean map of spatially high-pass filtered SST from the AMSR-E in Fig. 2d. These features significantly influence the overlying marine atmospheric boundary layer as shown by the co-location of surface wind speed anomalies from QuikSCAT and the SST anomalies (Fig. 2d), and their high correlation (Table 1).

Spatial variations in wind speed associated with cross-frontal changes in SST produce perturbations in the wind stress curl and divergence field related to perturbations in the crosswind and downwind

SST gradients (Chelton et al., 2001; O'Neill et al., 2003, 2005; Chelton et al., 2004). These curl and divergence perturbations have a dynamic range nearly as large as the background large-scale curl and divergence fields (O'Neill et al., 2003).

Correlations between near-surface winds and SST observed in satellite observations are consistent with limited in situ observations over the Agulhas Current and Agulhas Retroflection regions. Over the warm side of the Agulhas Current, surface latent and sensible heat fluxes increase dramatically (Jury and Walker, 1988; Mey et al., 1990; Jury, 1994; Rouault and Lee-Thorp, 1996; Rouault et al., 2000; Rouault and Lutjeharms, 2000), with measurements indicating as much as a factor of 5 increase (Jury, 1994). As winds blow from cool to warm water, increases in surface sensible and latent heat fluxes destabilize the boundary layer over the warmer water, enhancing vertical turbulent mixing, which deepens the boundary layer over the warmer water compared to cooler water. Boundary layer depth has been observed to change by as much as 300 m over the warmer water (Jury and Walker, 1988; Rouault et al., 2000). Cross-frontal boundary layer warming and deepening induces cross-frontal hydrostatic pressure perturbations, enhancing the cross-frontal surface flow from cooler to warmer water.

Observations over the Agulhas Current show that SST perturbations also affect low-level clouds. Cumulus and stratocumulus cloud decks are often seen to outline the position of the warmest waters of the Agulhas Current (Lutjeharms et al., 1986; Lee-Thorp et al., 1998; Lutjeharms and Rouault, 2000) upstream of the Agulhas Retroflection region. From radiosonde and satellite observations during the Agulhas Current Air–Sea Exchange Experiment (ACASEX), Lee-Thorp et al. (1998) concluded that cumulus convection over the Agulhas Current was associated with decreases in boundary layer stability and increases in surface sensible and latent heat fluxes over warmer water. Analysis of columnar-integrated cloud liquid water (CLW) from AMSR-E in the Agulhas Return Current region, showed that anomalies of cloud liquid water of around  $2 \times 10^{-2}$  mm were located about  $0.5^\circ$  downwind of SST anomalies. The magnitude of the anomalies could be explained by changes in stratocumulus thickness of a few hundred meters (O'Neill et al., 2005).

From case studies and model sensitivity analyses, ocean–atmosphere interactions over the Agulhas Current have a significant impact on regional rainfall and storm intensity over southern Africa (e.g. Reason, 2001; Rouault et al., 2003; Singleton and Reason, 2006). Large latent heat flux magnitudes over the core of the Agulhas Current enhance the precipitation over the southern portion of Africa (Rouault et al., 2003). In addition to supplying moisture to the overlying atmosphere, the SST structure of the Agulhas Current has been hypothesized to contribute to the location and intensity of a low-level wind jet, which funnels warm, moist air forming over the warmer waters of the Agulhas Current onshore (Singleton and Reason, 2006).

#### 2.4. Summary of MABL response to ocean fronts

The case studies described above, together with relevant studies of other regions, are used here to summarise the observed response of the MABL to ocean fronts.

##### 2.4.1. Surface

Surface roughness and stress are modified across fronts, such that rougher water is typically observed over warm SST. In addition to the cases described above, changes in surface roughness across ocean fronts have also been observed in other regions of the World's Ocean: including in the Southern Ocean (Belkin and Romanov, 1990), and in the Sargasso Sea (FASINEX: Friehe et al., 1991). The increase in stress can be due to changes in surface stability and/or wind speed, and is observed globally by scatterometer (Chelton et al., 2004) and by SAR (Sikora et al., 1995). In all cases, wind stress curl (divergence) anomalies are linearly related to the component of the background wind across (along) the fine scale SST gradients (Chelton et al., 2004).

##### 2.4.2. Stratification and cloud cover

Typically, stable or neutrally stable potential temperature profiles are observed over the cold side of fronts and unstable profiles over the warm side (e.g. in the eastern Equatorial Pacific), as might be expected from surface layer theory. These effects are actually felt much deeper in the boundary layer,

and substantial changes in surface heat fluxes across fronts give rise to changes in boundary layer structure and height. Deepening of the boundary layer over warm water has been noted by several authors (include [Sweet et al., 1981](#); [Wayland and Raman, 1989](#); [Kwon et al., 1998](#)). This situation will be complicated in mid-latitude regions where the passage of synoptic atmospheric features such as cold-air outbreaks may play a more important role in setting the stratification over short time scales. [Vihma et al. \(1991\)](#) noted that as well as synoptic events, the diurnal cycle also affects the near-surface stability over oceanic fronts.

In some cases, a shallow internal boundary layer (IBL) is formed as air flows across a front. An IBL, which forms inside the pre-existing deeper boundary layer, can take the form of a shallow stable layer or unstable mixed layer depending on the sign of the air-sea temperature difference. This has been observed in the case of warm to cold water ([Rogers, 1989](#)), where the IBL restricted the exchange of fluxes from surface to upper boundary layer. Also, for air flowing from cold to warm water, a shallow unstable IBL was observed to form across the Kuroshio ([Hsu, 1984a](#); [Tokinaga et al., 2006](#)), and across the equatorial Front ([Anderson, 2001](#); [Hashizume et al., 2002](#)).

Warming and deepening of the boundary layer causes increased amounts of low-level cloudiness over the warm downwind side of SST fronts. Changes in cloud cover are observed, for instance in the warm sector of tropical instability waves ([Deser et al., 1993](#)), and along the line of the Gulf Stream ([Fig. 7b](#)), and over the Agulhas Return Current. These clouds develop partly in response to the latent heat flux changes across the front, with turbulent eddies transporting moisture towards cooler air above, as well as through organized ascent in secondary circulations. In the EPIC section across the Equatorial Front at 95°W, cloud-topped boundary layers (more precisely, stratocumulus and the occasional penetrating cumulus congestus) were found to be co-located with the region of maximum surface latent and sensible heat fluxes. Over the Gulf Stream, 'sea-smoke' rising from the seas surface has been observed and seen occasionally to link with particularly low cloud bases, presumably a sign of convective plumes ([Wayland and Raman, 1989](#)). In contrast over the Cold Tongue, surface fog has been observed where warm moist air is advected across the cool surface (Nick Bond, personal communication). In FASINEX [Rogers \(1989\)](#) noted that surface forced clouds were present over warm water but over cold water the stable internal boundary layer inhibited the turbulent exchange between surface and cloud layer.

#### 2.4.3. Wind profile

Changes of the surface wind due to SST were observed *in situ* and by satellites, but the perturbation to the wind extends much deeper, through the surface layer and the boundary layer. Observations over the eastern Equatorial Pacific show considerable wind shear over the cold water, and more uniform wind profiles over warm water, with the differences most marked over the lower 500 m ([McGauley et al., 2004](#), also [Fig. 4](#)).

In some observations notable jets form, within a few hundred meters of the surface, and these are referred to as low-level jets (LLJs). LLJs are a common phenomenon in reasonably stable boundary layers over land, where they are related to baroclinicity (via the thermal wind equation) induced by weather systems, sloping terrain, and inertial oscillations ([Stull, 1988](#)). (The LLJ over land often becomes stronger at night when turbulence reduces near the cold land surface, and momentum is not transferred to the surface but remains above in a nocturnal jet.) Similar jets have been observed near oceanic SST fronts. [Vihma et al. \(1998\)](#) noted the presence of LLJs in 90% of rawinsonde soundings in a 4 weeks cruise at the Denmark Strait, which were most strong either when background flow was along the front, so that the change in air temperature across the SST front enhanced the jet via thermal wind, or when warm air was advected over a cold surface (akin to the nocturnal jet case mentioned above), or when flow originated from the steep topography of Greenland (possibly due to the upstream orographic influence on baroclinicity also discussed above). [Wayland and Raman \(1989\)](#) detected a LLJ over the Gulf Stream at about 100 m height related to the baroclinic gradient.

In some observational studies the wind profile changes have been described as part of an ageostrophic secondary circulation. In SEMAPHORE, an experiment that took place close to the Azores Front in 1993 ([Eymard, 1998](#)), considerable importance was given to the existence of ageostrophic winds as part of a thermally direct circulation cell. Marine boundary layer warming by surface sensible heat fluxes that arise from the SST change over a short distance appears to be the major contributor

to the secondary circulation cell (Kwon et al., 1998; Giordani et al., 1998). In particular an increase of wind speed from the cold to the warm side of the front was attributed to these effects (Giordani et al., 1998). Earlier Khalsa and Greenhut (1989) detected a secondary circulation induced by an SST front southwest of Bermuda in FASINEX.

### 3. Numerical models and mechanisms of atmospheric response to fronts and eddies

The case studies above suggest that there is some consistency in physical processes of air-sea interaction occurring in the three case study regions, despite their differing atmospheric and oceanic environments (trade wind regime vs. mid-latitude storm track: equatorial upwelling regime vs. warm western boundary current, northern vs. southern hemisphere). In this section we describe how numerical models and theoretical concepts have been used to help understand these processes. Specific numerical simulations are described first in Section 3.1, followed by a discussion of the mechanisms derived from these and simpler models in Section 3.2. Section 3.3 and the accompanying schematic Fig. 15 summarise the findings.

#### 3.1. Numerical simulations

Here previously published model experiments are divided by model type, namely idealized models, boundary layer models, and 3-D regional or mesoscale models. Although there are other useful ways of classifying the modeling (e.g. steady flows vs. time varying, or two-dimensional (vertical slice) vs. three-dimensional) this chosen classification is useful in describing the physical mechanisms in different levels of complexity.

##### 3.1.1. Analytical and idealized models

Hsu (1984b) modeled the response to the Gulf Stream SST front in terms of a sea-breeze response to the change in surface heat fluxes across the front. In this model, the well-mixed boundary layer potential temperature is estimated as equal to the SST, and the boundary layer pressure is derived from the air temperature. The derivation is similar to that for the real sea-breeze (based on the Circulation theorem; Holton, 2004), except that the Gulf Stream warm water is the 'land', the slope waters the 'sea', and there is no significant diurnal cycle. The difference in air temperature on either side of the front leads to pressure gradients which drive the flow (similar to the concept used to model the response to large-scale tropical SST gradients by Lindzen and Nigam, 1987). Using empirically derived frictional coefficients in a simple  $k$  formulation Hsu (1984b) obtained a wind speed change of 8 m/s across the front. This simple model gives a qualitatively good solution (compared with data from Sweet et al., 1981), for certain reasonable values of  $k$ . Sublette and Young (1996) hypothesized that this type of sea-breeze effect may be quite appropriate in summer off North Carolina when the prevailing winds are typically along the Gulf Stream Front, hence not interfering with the cross-front atmospheric circulation. Indeed they observed a cloud band close to the Gulf Stream north wall which may be forced by the upward part of the sea-breeze cell deepening the MABL.

A model of the internal boundary layer height change due to flow across a surface temperature gradient was formulated from first principles by Venkatram (1977).<sup>6</sup> The model may be written as (Hsu, 1984a)

$$h = \left( \frac{2C_D(\theta_{\text{warm}} - \theta_{\text{cold}})X}{\gamma(1 - 2F)} \right)^{1/2} \quad (1)$$

where  $h$  is internal boundary layer height,  $C_D$  the drag coefficient,  $\theta_{\text{warm}}$  and  $\theta_{\text{cold}}$  the surface potential temperature on either side of a front,  $X$  is the distance or fetch downwind from the front,  $\gamma$  is the environmental lapse rate above the boundary layer and upwind of the front, and  $F$  is an entrainment coefficient. Hsu (1984a) and Anderson (2001) applied this formula to estimate the IBL height

<sup>6</sup> A related formulation for boundary layer height, based on surface fluxes, was designed by Gamo et al. (1983).

**Table 2**Estimates of IBL height  $h$  based on the model of Venkatram (1977)

Case	$C_D$	$\theta_{\text{warm}} - \theta_{\text{cold}}$ (K)	$X$ (km)	$\gamma$ (°C/m)	$F$	$h$ (m)
Kuroshio	0.0015	2.7	15	0.01	0.2	142
Equatorial front	0.0012	4	100	0.0096	0.2	355

Coefficients are explained in the text. The data from the Kuroshio is from Hsu (1984a), and that of the equatorial Front from Anderson (2001).

change across the Kuroshio front (in the Korea Strait) and across the Equatorial Front, respectively. Using parameter values estimated from observations (listed in Table 2) and an entrainment coefficient assumed to be 0.2 (based on Driedonks, 1982), the IBL height was found to be 142 m and 355 m over the Kuroshio and Equatorial Front, respectively, in reasonable agreement with observations (Hsu, 1984a; Anderson, 2001).

Riordan and Lin (1992) modeled the wind response to the Gulf Stream in terms of the forcing by shallow diabatic heating. This linearised, hydrostatic model included advection by the mean flow and was solved analytically by means of Fourier Transform. The diabatic heating due to air flowing across the Gulf Stream was modeled as a shallow source with an  $e^{-z/H}$  vertical dependence and an e-folding scale of 1 km. The model was used to interpret the observed patterns of diffusione and confluence in coastal fronts occurring during GALE in winter, and was forced by heating with a horizontal pattern based on that observed (Riordan and Lin, 1992).

Bourras et al. (2004) used the Sawyer–Eliassen equations to analyze the ageostrophic response in a full three-dimensional model. The Sawyer–Eliassen equations describe the time evolution of the thermal wind *imbalance* term ( $f(\partial u / \partial z) + (\partial b / \partial y)$ , where  $b$  is the buoyancy), which is zero in the geostrophic case due to thermal wind, and is non-zero when there is an ageostrophic component. They conclude that the momentum-mixing term is the primary factor in maintaining the thermal wind imbalance and an anomalous secondary circulation in their full model (discussed below under Regional Models).

### 3.1.2. Boundary layer models

Koračin and Rogers (1990) applied a one-dimensional model of the marine boundary layer to study the response to a gradual change in SST. Based on the Mellor–Yamada turbulence closure, this type of model is designed to study mixing processes in detail but cannot include advective and SST induced pressure gradient effects. Investigating the response to a temporal change of surface forcing from warm to cold water, Koračin and Rogers (1990) detected the formation of a stable IBL over the cold water, as well as the development of LLJs. In the stable IBL, a reduction of the turbulent moisture flux lead to a decoupling of surface and cloud layer so that the cloud amount was significantly reduced from that over warmer water. They also noted the additional influence of the diurnal cycle: solar radiation in daytime heats the cloud layer and causes decoupling from the surface.

Two-dimensional boundary layer models were employed by Huang and Raman (1988) and Wai and Stage (1989) to investigate the occurrence of cold-air outbreaks flowing across the Gulf Stream front. In these types of simulations the investigation is essentially of a steady flow, with some fixed initial values of velocity and temperature profiles given, upstream of the Gulf Stream. Both papers note a significant convergence and vertical motion associated with the Gulf Stream. The location of the surface convergence depended on the strength of the background geostrophic wind: stronger winds lead to convergence further downstream of the SST front (Huang and Raman, 1988). This effect may be considered as the influence of thermal advection: the maximum air temperature warming and mixed layer deepening occurs further downstream under stronger winds.

Wai and Stage (1989) used a boundary layer model with level 4 turbulence closure to also show the existence of a secondary circulation cell with strongest surface flow at the front (towards the warm water), and a deeper mixed layer with clouds over the warm, rising portion. The model streamfunction (Fig. 9) illustrates the secondary, cross-frontal, circulation. Their analysis of the cold-to-warm sea surface temperature (SST) case showed that, in addition to enhancement of vertical mixing in the MABL when the air mass is advected from the cold to the warm side, the pressure gradient force

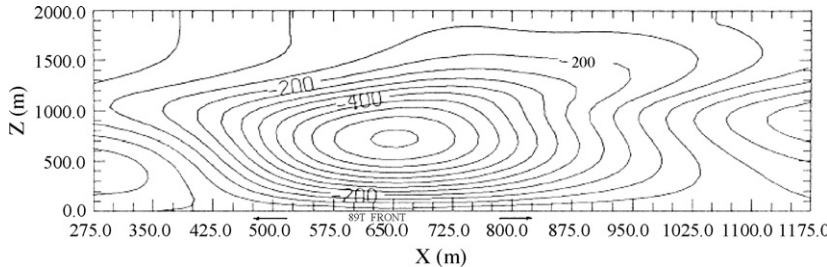


**Fig. 9.** Contours of perturbation streamfunction ( $\text{m}^2 \text{s}^{-1}$ ) from a numerical simulation of boundary layer flow across the Gulf Stream. The figure shows a distance–height cross-section with total range of 900 km (x, abscissa)  $\times$  2000 m (z, ordinate). The location of the idealized SST front is shown on the abscissa, where SST increases from 6 °C on the left hand side to 19 °C on the right, over a distance of 350 km. The specified initial wind is an Ekman spiral corresponding to a geostrophic wind of  $10 \text{ m s}^{-1}$  crossing the front at an angle of 45°. The streamfunction anomaly corresponds to upward motion to the right of the front, centered at 800 km, and downward motion to the left of the front centered at 475 km. The strongest near-surface wind speeds of over  $10 \text{ m s}^{-1}$  are found above the front. From Wai and Stage (1989). Reproduced with permission of John Wiley and Sons Ltd., on behalf of RMETS.

is important in the momentum budget. In particular they showed that the change in surface stress across the front is dominated by the change in pressure-driven winds rather than by the change in drag coefficient due to stability changes.

Recently the explicit resolution of turbulent eddies of  $O(100 \text{ m})$  scale in the boundary layer has been studied using Large Eddy Simulations (LES). Here, typically, high resolutions of  $O(10 \text{ m})$  or less are afforded in relatively small domains of a few km or less horizontally or vertically. Whilst the turbulent fluxes due to large eddies are treated explicitly, sub-grid parameterisations are used to model turbulence on scales even finer than the model resolution.

LES models have added to our understanding of processes at the Equatorial Front. deSzeoeke and Bretherton (2004) used a quasi-Lagrangian LES model to track the progress of air parcels being advected with the mean wind across the SST front at 95°W. The LES predicted the vertical structure of a boundary layer column under horizontally homogeneous large-scale forcing. Grid spacings were 50 m in the horizontal and 25 m in the vertical. The model equations included terms prescribing large-scale forcing, namely the pressure gradient and advection by the mean zonal wind from NCEP/NCAR reanalysis. The SST surface boundary condition was idealized from TRMM satellite Microwave Imager (TMI) retrievals.

The LES model of deSzeoeke and Bretherton (2004) shows the development of a mid-boundary layer jet at around 300 m height, due to the background pressure gradient, over the cold tongue (Fig. 10a). In this stable environment there is strong shear and weak surface wind, corresponding to the low surface drag. As the front is reached, there is a rapid redistribution of momentum in the lower boundary layer and the surface wind increases by  $1.5 \text{ m s}^{-1}$  in 1 h or over just 20 km (Fig. 10a and c). The surface acceleration coincides with a peak in TKE in the lowest 200 m (Fig. 10b), and a rapid increase in surface heat fluxes (Fig. 10d). Integrated over the depth of the boundary layer, the meridional velocity actually decelerates, due to the increased drag. These results, together with explicit calculation of the momentum budget indicated that here the vertical transfer of momentum by mixing is accelerating the surface flow (deSzeoeke and Bretherton, 2004).

Further LES simulations by Skillingstad et al. (2007) explored the MABL response to flow across different types of fronts, in particular for warm to cold SST changes (WC) and also for cold to warm (CW). The SST changes are steps, separated by 10 km sections of uniform SST. SST values were from 15 to 19 °C, representative of mid-latitude oceans. The vertical size of the domain was relatively small (200 m) allowing very high resolution of 4 m in all directions. For the WC case, an IBL of  $O(10 \text{ m})$  was formed immediately downwind of the cold SST, associated with a drastic reduction in turbulence, low surface drag and a high velocity shear between low surface winds and stronger winds aloft. When the IBL is advected across a warm ocean in the CW experiment, strong convective mixing destroyed the IBL giving rise to an unstable environment with much higher surface winds and low wind shear. For these

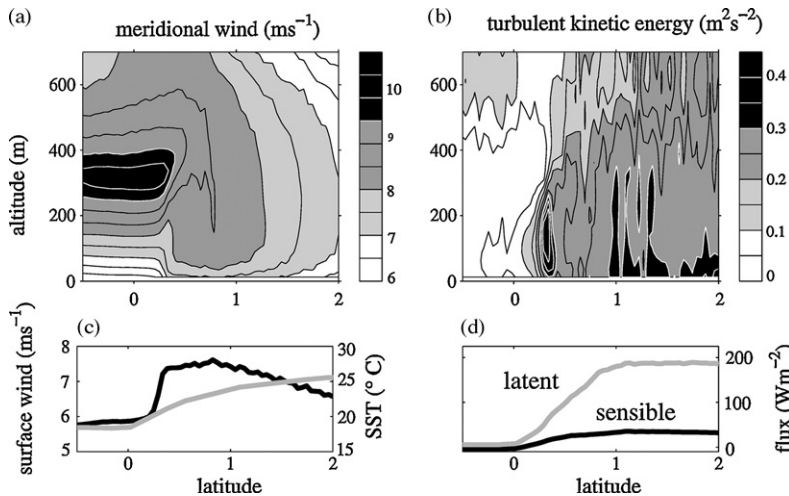


**Fig. 10.** The transition of the lower MABL as the MABL crosses the SST front, from a Large Eddy Simulation (LES). The left panels show the meridional wind in (a) vertical section and (c) at surface, and the right panels show (b) the TKE in vertical section and (d) heat fluxes at the surface. Here the SST front occurs mostly between the equator and 1°N, where SST changes from 18.5 to 24°C (shown as a grey line in (c)). Note the abrupt increase in near-surface meridional wind, TKE, and heat fluxes at the front. From deSzeke and Bretherton (2004). Reproduced by permission of the American Meteorological Society.

simulations, examination of the momentum budget indicated that as in the deSzeke and Bretherton (2004) experiments, the changes in stratification and wind were driven by the changes in momentum flux, with negligible pressure gradient terms.

### 3.1.3. Three-dimensional regional or mesoscale models

Fully three-dimensional models have also been applied to study the response of atmospheric boundary layers to ocean fronts. Although some studies of TIWs have been performed using global circulation models (Xie et al., 1998), their coarse resolution generally provides poor resolution of oceanic frontal zones. More extensive use has been made of regional atmospheric models (RAMs) for high resolution studies of regions of interest, constrained by boundary forcing by global models or reanalyses. Examples of these include Pennsylvania State University-National Center for Atmospheric Research (NCAR) Mesoscale Model (MM5) and its successor Weather Research and Forecasting (WRF, Skamarock et al., 2005), the Naval Research Laboratory Coupled Ocean-Atmosphere Prediction system mesoscale atmospheric model (COAMPS, Hodur, 1997), the Experimental Climate Predictions Center and National Centers for Environmental Prediction (NCEP) regional spectral model (Juang et al., 1997) and the International Pacific Research Center (IPRC) RAM (Wang et al., 2003).

The RAMs can be used to model time varying flows in three-dimensions with constrained large-scale motion but freely evolving small-scale air-sea interaction. Some early simulations were performed to study the atmospheric response to the Gulf Stream to support the GALE Experiment (Dirks et al., 1988). Warner et al. (1990) and Doyle and Warner (1993) performed numerical modeling experiments to study the impact of SST resolution on mesoscale coastal processes, and they found that the MABL structure is very sensitive to the SST distribution. From their simulations, a secondary circulation, ascending over the warm water and descending over the cold water across SST fronts was found, similar to that found in the boundary layer models of Huang and Raman (1988) and Wai and Stage (1989). Sublette and Young (1996) used MM4 to interpret observations of a cloud band over the Gulf Stream North Wall in summer, finding that the model reproduced the cloud band, but in a slightly different location, over the warmest SST rather than over the Wall (the SST gradient region).

A number of studies of the response of extra-tropical cyclones to ocean fronts, in particular the Gulf Stream, have been performed. The surface flux changes that occur across the ocean fronts appear to help the growth of storms and/or steer developing storms (Kuo et al., 1991; Xie et al., 2002; Businger et

al., 2005; Sampe, 2005; Minobe et al., 2008). Reed et al. (1992) describes the storm evolution in terms of the roles of the low-level baroclinic zone and an upper level potential vorticity anomaly (PVA), and how diabatic heating adjusts the PVA. Businger et al. (2005) noted that the diabatic heating associated with the latent heat release in the storm formed a mesoscale geopotential height anomaly aloft, which led to acceleration of the flow and increased mass divergence above the surface cyclone.

A number of more recent RAM studies of the responses to fronts and eddies have been motivated by the results and hypotheses arising from new satellite data and field programs described in Section 2. These include studies of the Equatorial Front (Small et al., 2003, 2005b), of central North Atlantic fronts (Bourras et al., 2004; Song et al., 2004), and of the Gulf Stream (Song et al., 2006), which are described next.

The atmospheric flow over TIWs has been studied using the IPRC RAM, forced by a time-evolving SST field taken from TMI observations (Small et al., 2003). Regressions of the model high-pass filtered near-surface winds onto the SST variability due to TIWs showed similar characteristics to those observed by satellite (compare Fig. 5a and b). Regression of other model variables onto the same SST timeseries revealed an interesting feature: the sea level pressure response was lagged downstream of the SST in the direction of the mean wind. The near-surface winds essentially flowed down the pressure gradient (as the Coriolis force is negligible at these latitudes). The downstream shifting of the pressure gradients, as well as their magnitude, was consistent with the analysis of EPIC barometer data by Cronin et al. (2003) reported in Section 2.1.

Small et al. (2005b) extended this work to study the time-mean cross-equatorial flow in the EPIC region. As in the deSzeoek and Bretherton (2004) LES model and the observations, the RAM predicted large increases of sensible ( $30 \text{ W m}^{-2}$ ) and latent heat flux ( $150 \text{ W m}^{-2}$ ) across the front as the air changed from stable conditions over the cold tongue to unstable over the warmer waters north of the front. The wind stress also increased across the front. A detailed analysis of the RAM momentum budgets revealed that again the change in surface wind was due to an induced pressure gradient, part of an anomalous secondary circulation in the boundary layer. This result is an important modification to the theory of Lindzen and Nigam (1987) in that the advection of temperature by the mean wind in the RAM causes the pressure gradient to be located downstream of the SST gradient. As shown in the  $95^{\circ}\text{W}$  cross-section from model and observations (Fig. 11), the peak SST gradient is narrow and centered on the equator (Fig. 11a), whereas the surface air virtual temperature gradient peak is broader (Fig. 11b), and the surface pressure gradient peaks between  $3$  and  $4^{\circ}\text{N}$  (Fig. 11c), which is where the strongest meridional winds are observed (Fig. 11d: the winds veer thereafter and have a stronger zonal component under the influence of rotation). The inclusion of advection removes the main criticism by Hayes et al. (1989) of the Lindzen and Nigam (1987) mechanism, that *co-located* SST and pressure gradients cannot explain the observed wind divergence. Instead the downstream location of the observed and RAM modeled pressure gradient can give rise to pressure gradient driven winds that diverge across the front.

The role of secondary circulations in the interaction process was also studied by Bourras et al. (2004), concerning flow over a cold eddy observed in the North Atlantic. Consistent with all previous studies, reduced scatterometer winds were found over the cold eddy. On applying the MM5 regional atmospheric model to the observed SST field, and comparing against a model run with a smooth SST field, they noted that an anomalous secondary circulation was set up, which was analysed using the Sawyer–Eliassen equations as discussed above.

Song et al. (2006) studied the effect of the Gulf Stream SST front on the wind flow by a joint quantitative analysis of the NASA Ku-band scatterometer (NSCAT) and QuikSCAT scatterometer-derived winds, AVHRR SST data, and MM5 simulations. The MM5 model was run with the Medium-Range Forecast (MRF) (Hong and Pan, 1996)<sup>7</sup> MABL scheme, following results from a preliminary study (Song et al., 2004), which showed that the MRF provided the best representation of the MABL over an SST front observed in FASINEX (Friehe et al., 1991). The MABL model was further modified by Song et al. (2006) to allow the incorporation of the Gulf Stream current as part of the bottom boundary condition

<sup>7</sup> The MRF scheme uses a Richardson number dependent vertical diffusion coefficient together with a parameterization of non-local turbulence from large eddies (Hong and Pan, 1996).

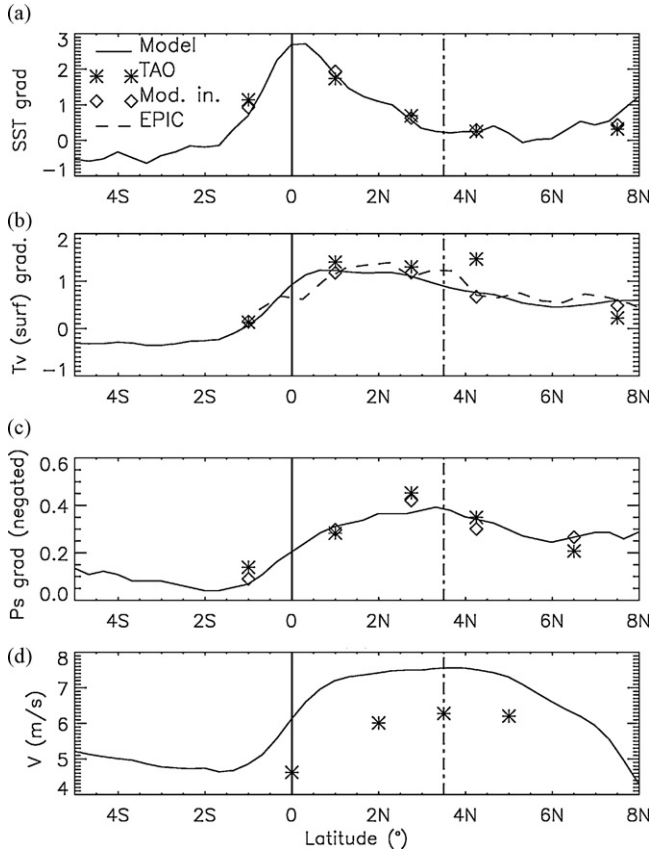


**Fig. 11.** Cross-section of surface properties at 95°W, in the eastern tropical Pacific, averaged between September and October 2001. Data from the 8 flight NCAR C130 composite (EPIC2001), TAO moorings and the IPRC Regional Atmospheric Model (see legend). (a) Meridional gradient of SST (K per 100 km), (b) meridional gradient of near-surface virtual temperature (K per 100 km), (c) meridional gradient of surface pressure, negated (hPa per 100 km), and (d) neutral 10 m meridional wind ( $m s^{-1}$ ), from model and TAO. Gradients derived from model data sampled at TAO mooring positions are also shown (diamonds). The thick vertical line marks the equator, close to the latitude of the peak SST gradient, and the thick chained vertical line marks the approximate latitude of highest meridional wind in observations and model, around 3.5°N. Adapted from Small et al. (2005b). Reproduced by permission of American Meteorological Society.

(refer to (2)). Song et al. selected special cases from the satellite data which showed nearly steady winds flowing across the SST front, either from cold to warm or vice versa. This was then studied in a three-dimensional model framework, but with a model set-up which was essentially two-dimensional, with the wind flow steady and perpendicular to an idealized, straight front with properties estimated from the satellite data.

Preliminary experiments with the MM5 model showed that non-hydrostatic effects (vertical accelerations) became important when the grid spacing was reduced to around 15 km or less. Noting that large changes in SST can occur over these kinds of length scales, Song et al. (2006) applied the MM5 in non-hydrostatic mode with resolutions as high as 5 km, to show that the perturbation pressure gradient is the main force modifying the air flow across the front. When the wind blows from cold to warm water across an SST front, strong mixing homogenizes the entire MABL downwind of the front (Fig. 12a and b). This, together with an increase in the mean temperature of the MABL, leads to low and high perturbation pressure anomalies from the ocean surface to the upper part of the MABL (Fig. 12c). Specifically, there is a negative perturbation pressure anomaly near the surface over, and immediately downwind of, the front and a positive perturbation pressure anomaly aloft within the

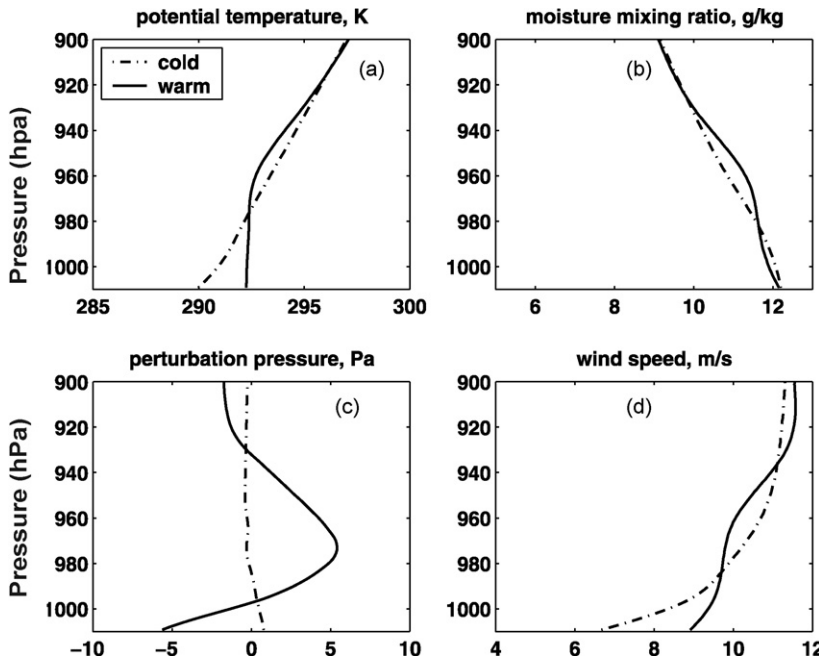


**Fig. 12.** Flow across the Gulf Stream in a cold to warm case from a Regional Atmospheric Model simulation. The plots show the profiles over the warm water and over the cold water (see legend). (a) Potential temperature (K), (b) moisture mixing ratio ( $\text{g kg}^{-1}$ ), (c) perturbation pressure difference (Pa), and (d) wind speed ( $\text{m s}^{-1}$ ). From Song et al. (2006). Copyright American Geophysical Union (2006) and reproduced by their permission.

MABL.<sup>8</sup> The resulting surface pressure gradient gives rise to stronger surface winds over the warm water but weaker winds aloft (Fig. 12d). The surface wind divergence draws air into the MABL from the free atmosphere giving rise to a modification of the free atmosphere that extends well upwind and downwind of the front. When the wind blows from warm to cold (Fig. 13), the underlying cold water tends to stabilize the MABL and a stable internal boundary layer (IBL) was formed downwind of the front that reduced the vertical exchange of air in the MABL. This, together with a decrease in the mean temperature of the MABL downwind of the front, resulted in a high and a low perturbation pressure anomaly between the ocean surface and the upper part of the MABL, a reverse dipolar pattern of perturbation pressure downwind of the front in contrast with what was found in the cold to warm case.

The RAM experiments listed above were designed for case studies where direct comparison with observations could be made. This necessarily limits the range of scenarios that could be addressed. A more recent study by Spall (2007a) has considered a fuller range of idealized situations, focusing more on the mechanics of the interaction rather than the validation against observations. Using the coupled COAMPS/Regional Ocean Model (ROMS) of Perlin et al. (2007, see Section 4.3 and Table 3), the MABL response to ocean fronts was examined in a 2-D situation. These experiments included a discussion of the sensitivity to upstream wind speed, Coriolis force (latitude), and direction of SST gradient. The results revealed much about the mechanisms of atmospheric response and are included in the following sub-section.

<sup>8</sup> The reason for this is simply explained, e.g. for the case of cold to warm water when the MABL is deepened. Below the original boundary top (usually marked by a layer of strong stratification and inversion), the increase in temperature over the warm eddy implies a reduction in density. Meanwhile, above the original top of the MABL, the new deeper MABL gives an anomalous increase in density (as relatively heavy MABL intrudes into the lighter free atmosphere). This results in a dipole of pressure anomalies in the vertical: positive above and negative below.

**Table 3**

Regional coupled models, with some details of the model grids, domains and simulation times

Authors	Atmospheric model				Ocean model				Simulation time
	Name	Horizontal resolution (km)	#Vertical levels	Domain	Name	Horizontal resolution (km)	#Vertical levels	Domain	
Xue et al. (2000)	ARPS	10	34	2-D, 640 km × 12 km high	POM	10	51	2-D, 500 km × 3 km deep	A few days
Li et al. (2002)		20	26	3-D, 2400 km square, 18 km high		10–15	26	3-D, about 2000 km square × 4.5 km deep	A few days
Perlin et al. (2007)	COAMPS	1	47	3-D, 50 km × 20 km by 9 km high	ROMS	1	40	3-D, 50 km × 20 km by 300 m deep	3 days
Spall (2007a)		4	47	2-D, 800 km × 9 km high		4	25	2-D, 800 km × 500 m deep	2 days
SCOAR Seo et al. (2007a,b)	NCEP RSM	20–50	28	3-D, 1000–4000 km square, whole column	ROMS	10–50	20	3-D, 1000 km square or 4000 km square, full ocean depth	5 years
IROAM Xie et al. (2007a)	IPRC RAM	50	28	3-D, 12000 km × 7000 km, whole column	MOM2	50	30	3-D, Pacific basin between 35°N and 35°S, by 4 km deep	8 years

Here ARPS denotes Advanced Regional Prediction System (Xue et al., 1995), POM the Princeton Ocean Model (Blumberg and Mellor, 1987), ROMS: the Regional Oceanic Modelling System (Shchepetkin and McWilliams, 2005), COAMPS the Naval Research Laboratory Coupled Ocean/Atmosphere Mesoscale Prediction System (Hodur et al., 1997), NCEP RSM is the Experimental Climate Predictions Center and NCEP regional spectral model (Juang et al., 1997), MOM2 the Geophysical Fluid Dynamics Laboratory Modular Ocean Model (Pacanowski and Griffies, 2000), IPRC RAM the International Pacific Research Center IPRC regional atmospheric model, IROAM is the International Pacific Research Center regional ocean atmospheric model, and SCOAR is the Scripps Coupled Ocean Atmosphere Regional Model.

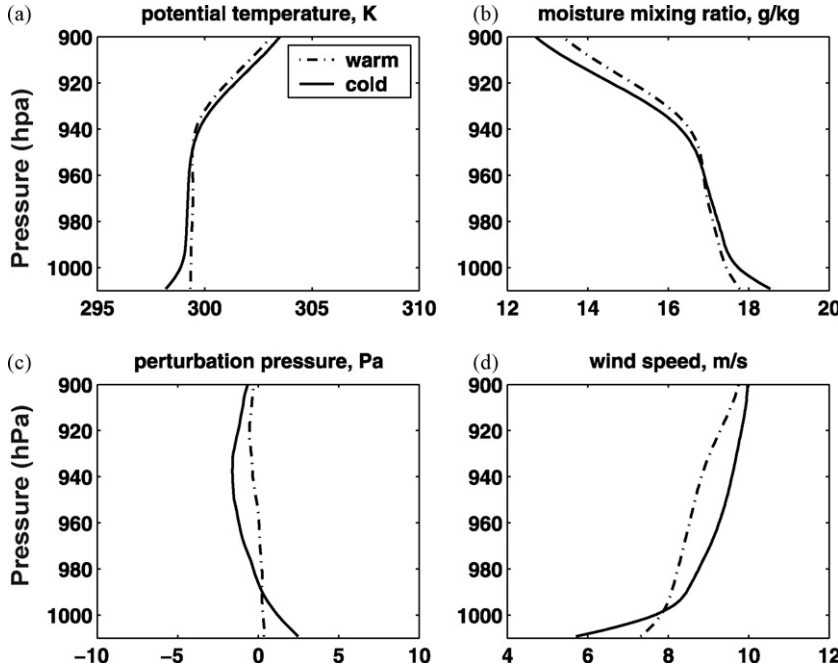


**Fig. 13.** Flow across the Gulf Stream in a warm to cold case from a Regional Atmospheric Model. The plots show the profiles over the warm water and over the cold water. (a) Potential temperature (K), (b) moisture mixing ratio ( $\text{g kg}^{-1}$ ), (c) perturbation pressure difference (Pa), (d) wind speed ( $\text{m s}^{-1}$ ). From Song et al. (2006). Copyright American Geophysical Union (2006) and reproduced by their permission.

### 3.2. Mechanisms of atmospheric response

The observations and numerical experiments described above have revealed a complexity to the air-sea interaction process that was not fully understood by some early investigators. In particular, the momentum mixing proposed by Wallace et al. (1989) and Hayes et al. (1989) to explain the phasing between SST and wind speed anomalies, is only one possible explanation. Various other effects not considered by these early investigators, including the effects of advection, pressure-driven secondary circulations, and changes to boundary layer height, can also give rise to the observed phase relationship.

In order to discuss the processes affecting the MABL response to SST fronts, it is useful to distinguish between the processes occurring in the frontal region itself, and those occurring upstream and downstream of the front where the SST is changing less rapidly. It appears that the former situation is more complex and not easily described by one simple process, whilst the latter situation is simpler and may explain some of the universal strong correlations between SST and MABL properties discussed in Section 1.

#### 3.2.1. MABL response to SST away from fronts

One of the expected features of the atmospheric response to different values of underlying SST is that the drag across the surface will change due to the change in surface stability. This is a basic feature of all bulk flux models (Liu et al., 1979; Fairall et al., 1996) which formulate the stress  $\tau$  as

$$\begin{aligned} \tau &= \rho_a C_D |U_{10} - U_c| (U_{10} - U_c) = \rho_a C_{DN} |U_{10N} - U_c| (U_{10N} - U_c) = \rho_a (u^*)^2 \\ C_D &= C_D (|U_{10N} - U_c|, T_s - T_a, q_s - q_a) \equiv C_D (z_0, \zeta) \end{aligned} \quad (2)$$

where  $C_D$  is drag coefficient,  $z_0$  the surface roughness length,  $u^*$  is the friction velocity,  $U_{10}$  the 10 m wind,  $U_c$  the surface ocean current,  $\rho_a$  atmospheric density,  $T$  the temperature,  $q$  the specific humidity,

$\zeta$  is a stability parameter ( $\zeta = z/L$  where  $z$  is height and  $L$  the Obukhov length), quantities underlined are vectors, and subscripts  $s$  and  $a$  denote sea and air ( $q_s$  is the saturation humidity over sea water at  $T_s$ ). For the moment the effect of ocean current  $\underline{U}_c$  is neglected, and it will be considered later in Section 4. The additional subscript  $N$  on the drag coefficient and 10 m wind denotes the neutral equivalent values. (With no current, there is a one-to-one relationship between the magnitude of  $U_{10N}$  and  $\tau$ .)

According to (2), the drag is a function of wind speed and surface stability and many studies have shown that the drag increases under more unstable conditions. This alone will lead to an increase in stress in unstable conditions (even if  $U_{10}$  is unchanged). The bulk flux formulation is part of the assumption of a constant-flux surface layer, and within this layer the wind speed profile takes the following form, based on the similarity theory of Monin and Obukhov (Liu et al., 1979; Stull, 1988):

$$|\underline{U}(z)| = \frac{u^*}{\kappa} \left( \ln \frac{z}{z_0} - \psi(\zeta) \right) \quad (3)$$

and similar formulations exist for air temperature and humidity. Here  $\psi(\zeta)$  is a stability function based on the Businger–Dyer model (Liu et al., 1979). Under neutral conditions, where  $\psi(\zeta) = 0$ , the wind speed takes the well-known logarithmic profile. Under stable conditions ( $\psi(\zeta) > 0$ ), the profile contains more shear near the surface than in the neutral case, whilst under unstable conditions ( $\psi(\zeta) < 0$ ) there is less shear. Hence, for a given value of  $U$  near the top of the surface constant-flux layer (e.g. at 100 m), the wind speed at 10 m will be higher in unstable conditions than in neutral conditions, and lower in stable conditions.

The surface layer theory outlined above has been used in the past to explain the link between SST and wind stress, assuming higher SST anomaly equates to more unstable conditions (which is typically, but not always, the case for ocean mesoscale features) (White and Annis, 2003). However, some papers have analyzed observations and model results to show that this effect can only make a minor contribution to the changes in wind stress (Wai and Stage, 1989; Small et al., 2003; O'Neill et al., 2005; Spall, 2007a). For instance, O'Neill et al. (2005) considered the effect on the stress of changing the value of the stability parameter  $\zeta$ . For a rather large range of  $\zeta$  from  $-0.3$  to  $0.3$ , and for a representative roughness length, the resulting change in wind stress was less than a third of that observed. It appears that some other effect is contributing to the changes in stress, namely a change in the wind speed above the surface layer.

Businger and Shaw (1984) hypothesized that the increased drag over warmer water will slow the winds down. However, the observations and models shown above all indicate that this is not the case. In fact it appears that the increase in drag over the warm water is not sufficient to slow down the winds which have been accelerated from cold to warm water under the mechanisms discussed below.

As expressed by the turbulent kinetic energy equation (Stull, 1988), turbulence can be generated away from the surface layer via shear production and buoyancy production, or it can be transported elsewhere by turbulent eddies. One consequence of this is that the surface buoyancy flux that occurs when air flows from cool to warm water can be transferred higher into the MABL by eddies, and can eventually act to deepen the boundary layer.

At this stage it is useful to consider the dominant terms of the momentum budget in the form

$$\underline{u} \cdot \nabla \underline{u} = -f \underline{k} \times \underline{u} - \frac{1}{\rho} \nabla p - \frac{\partial}{\partial z} \underline{u}' \underline{w}' \quad (4a)$$

I	II	III	IV
---	----	-----	----

where term I denotes horizontal advection, II is the Coriolis term, III the pressure gradient and IV the mixing term, with primes denoting turbulent quantities here. When vertically integrated over the boundary layer depth  $h$ , this becomes

$$\langle \underline{u} \cdot \nabla \underline{u} \rangle = -\langle f \underline{k} \times \underline{u} \rangle - \left\langle \frac{1}{\rho} \nabla p \right\rangle + \frac{\tau_e - \tau}{h} \quad (4b)$$

ADV	- COR	- G	STR. DIV.
-----	-------	-----	-----------

where angled brackets denote a depth average,  $\tau_e$  is the entrainment stress at the top of the boundary layer,  $G$  denotes the pressure gradient and the last term is the stress divergence. Samelson et al. (2006)

used the known sensitivity of boundary layer height to SST to derive a simple model of MABL response which is appropriate for the region away from the immediate frontal vicinity. Under the assumption that stress vanishes at the boundary layer top (so that  $\text{STR.DIV.} = -\tau/h$ ), and that advection and rotation are negligible ( $\text{ADV} = \text{COR} = 0$ ), a one-dimensional balance between pressure gradient and stress divergence leads to the relationship

$$\tau = -Gh \quad (5)$$

In this simple case the value of  $G$  is assumed not to change across the front. In other words surface stress  $\tau$  must increase with  $h$  for a given pressure gradient, because the stress divergence occurs over a larger vertical distance. This implies that under unstable conditions (warmer SST), when the boundary layer height increases through enhanced convection, the surface stress is larger, a relationship which is consistent with observations. Samelson et al. (2006) extended this analysis to a two-layer model including interfacial stress and rotation, and showed that in quasi-equilibrium conditions it was not possible to use interior boundary layer mixing (Wallace et al., 1989) to explain the observed dramatic surface wind changes. In the non-equilibrium case, where advection is important, the response depends on the ratio of the drag time scale to the advective time scale: when  $h$  is small the stress time scale is small and stress dominates; when  $h$  is large or the frontal width  $L$  is small then advection dominates (due to the strong gradients in wind and the large time for the boundary layer to fully respond to the stress, Samelson et al., 2006).

Spall (2007a) tested this 1-D balance in his coupled regional model. When the boundary layer height  $h$  was computed well downwind of the front, for scenarios of different background SST values, an approximate linear relationship was found between the change in  $h$  and the change in SST, supporting the 1-D balance. However, this relationship was found not to hold in the immediate region of the front. Reasons for this are discussed next.

### 3.2.2. MABL response in immediate vicinity of front

Some of the numerical investigations discussed above show results which are closely related to the early model of Lindzen and Nigam (1987). However, the original Lindzen and Nigam mechanism was designed for the response to large-scale SST features with weak gradients such that the air remained in equilibrium and advection could be ignored: but in the case of flow across a sharp SST front the strong gradients act to cause a rapid disequilibrium, and by the time a parcel of air in the boundary layer has completely responded to the SST change, it is well downstream of the front. Models of Huang and Raman (1988) and Small et al. (2005b) show that this results in maximum air temperature perturbation downstream of the front, together with the hydrostatic pressure anomaly.

The effects of background advection have been studied in more detail in a numerical framework by Spall (2007a). In a two-dimensional situation of flow across a front from cold to warm SST, the upstream wind speed was varied between experiments. It was found that the surface wind speed increased as the front was crossed in all the experiments, but the mechanisms governing the acceleration were fundamentally different for high background wind speeds than for low wind speeds.

### 3.2.3. Thermal advection

Thermal advection is important in determining the amount to which an air parcel adjusts to an SST front, and the length scale of adjustment. Under an advective–diffusive balance for zonal flow,

$$u \frac{\partial \theta}{\partial x} \sim - \frac{\partial}{\partial z} \overline{\theta' w'} \quad (6a)$$

Vertically and horizontally integrating gives

$$\langle \Delta \theta \rangle \sim \int_0^X \frac{H}{\rho_a c_p h} \frac{dx}{\langle U \rangle} \quad (6b)$$

where  $H$  is the sensible heat flux, and  $c_p$  the specific heat capacity of air. Here it is assumed that the air within the boundary layer is all moved at the depth-averaged velocity  $\langle U \rangle$  (Vihma et al., 1998; Small et al., 2005b). When wind speeds are high, air parcels have little time to adjust to the underlying surface temperature, such that the change in air temperature over a given distance is much smaller than

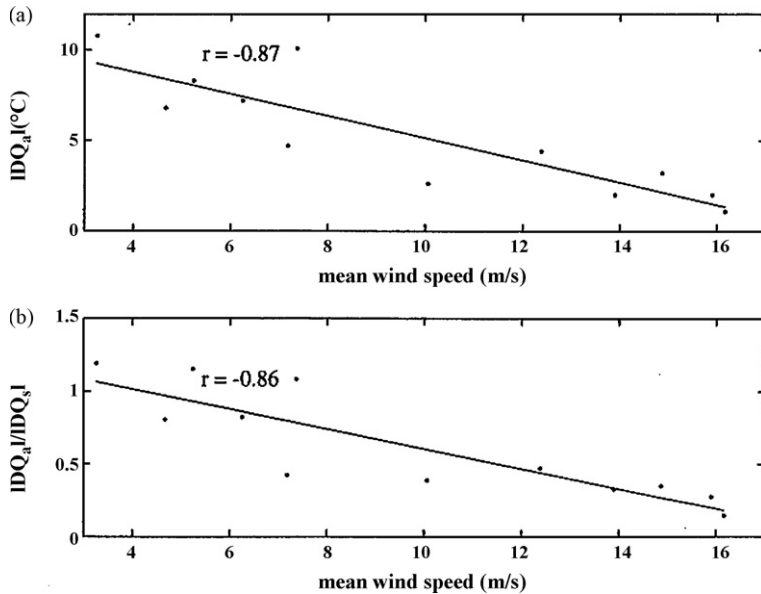


**Fig. 14.** Effect of wind speed on the (a) cross-frontal change in the air temperature  $|\Delta\theta_a|$  and (b) ratio of cross-frontal change in air to that of sea surface temperatures  $|\Delta\theta_a|/|\Delta\theta_s|$ , based on ship meteorological data from a front in the Denmark Strait. The abscissa represents the mean wind speed during each of the major frontal crossings (cases with the wind parallel to the front are not included). From Vihma et al. (1998). Copyright American Geophysical Union (1998) and reproduced by their permission.

the change in SST. In contrast, under low wind speeds, the air parcels adjust more to the underlying temperature and larger air temperature contrasts are observed across fronts (Fig. 14, from Vihma et al., 1998). Another consequence of this is that air-sea temperature differences will be larger under high wind conditions.

Alternatively, the length scale of adjustment can be derived in terms of the eddy diffusion coefficient  $K_T$  (Spall, 2007a). Writing

$$\begin{aligned}
 -\frac{\partial}{\partial z} \overline{\theta' w'} &= \frac{\partial}{\partial z} \left( K_T \frac{\partial \theta}{\partial z} \right), \text{ then} \\
 u \frac{\partial \theta}{\partial x} \sim \frac{\partial}{\partial z} \left( K_T \frac{\partial \theta}{\partial z} \right) &\text{ scales to} \\
 U \frac{\Delta \theta}{L_p} \sim \frac{1}{h} \left( K_T \frac{\Delta \theta}{h} \right) &\Rightarrow L_p = \frac{Uh^2}{K_T},
 \end{aligned} \tag{7}$$

the length scale  $L_p$  in (7) may be approximated as the length scale over which the pressure (a vertically integrated function of temperature) also changes. For high upstream wind speeds, and/or deep boundary layers, the length scale over which the pressure changes is long, and the induced pressure gradient is small. For weak winds the air temperature changes over similar scales as the SST.

### 3.2.4. Relative roles of pressure gradient, mixing, and Coriolis terms

The importance of the pressure gradient, mixing and Coriolis terms in the momentum budget is partly governed by the typical length scales for each term, and how they compare with the length scale of the front,  $L_f$ . In addition to the length scale for the pressure gradient term given by (7), the length scale over which the Coriolis term II changes is given by  $U/f$  (as seen by scaling the momentum budget (4a), under a balance between advection and Coriolis force). In conditions of strong advection, the length scales over which the pressure gradient and Coriolis terms change are long ( $U/f \gg L_f$ ,  $L_p \gg L_f$ ).

Consistent with this scaling, Spall (2007a) found that terms I and IV of (4a) underwent most changes in the boundary layer when a front was crossed under high background wind speeds. In particular, for a simulation of air flowing from warm to cold, an increase in the stress divergence (term IV), due to a reduction in boundary layer height over the cold water, acted to decelerate the flow in the lower boundary layer. In contrast, for flow from cold to warm water, the stress divergence term reduced to near zero or even changed sign over the warm water, due to the sudden increase in mixing and boundary layer height. This dramatic change left the Coriolis term unbalanced and led to an acceleration of the flow (equivalently to a change in the advection term I). In the upper boundary layer, for the cold to warm case, the flow was decelerated as the stress divergence became larger and acted against the flow. Spall (2007a) explained the acceleration at low levels and deceleration above not as a redistribution of momentum by the turbulent mixing, but rather as an exchange of momentum with the meridional flow when the Coriolis force becomes unbalanced.

In contrast to the above cases, for weak advection, the pressure changes over length scales comparable with the front ( $L_p \sim L_f$ ,  $U/f \sim L_f$ ), so that term III also becomes important in the frontal region. In this case Spall (2007a) noted that the pressure gradient could drive the acceleration from cold to warm water, with the mixing term IV acting as a drag, as found by Small et al. (2005b) and Song et al. (2006).

Samelson et al. (2006) also noted that for the case of air flowing from a cold to a warm surface, under strong advection, turbulent mixing is enhanced within a deepening boundary layer (or IBL) over the warm water, and momentum can be transferred from the surface, accelerating the flow there. However, they argue that for flow from warm to cold, a direct transfer of momentum cannot be responsible for the reduction of wind speed. It seems that either the simple balance (5) or the transfer of momentum from zonal to meridional flow (Spall, 2007a) is responsible for the reduction of winds in this case.

### 3.2.5. Modification of boundary layer height

It should be noted that changes in the boundary layer height, due to turbulent buoyant fluxes, will not only modify the stress divergence but will also affect the pressure gradient. For example, consider an idealized boundary layer with air of a uniform density, below a free troposphere of lighter air. Deepening the boundary layer (and consequently increasing the vertical integral of  $\rho$ ) will then increase the surface pressure. Hence, when computing the pressure change for air flowing from cold to warm surface, there will be some cancellation between the effects of heating of the boundary layer (which will reduce the pressure) and of the deepening of the boundary layer (which will increase the surface pressure).

### 3.2.6. Interpretation of differences in model results

The models of Samelson et al. (2006) and Spall (2007a) may be used to help interpret and synthesise the observations of Section 2 and the model results of Section 3.1. Firstly, the observed correlation of wind stress magnitude and SST follows the Samelson et al. observation that deeper boundary layers are associated with higher surface stress in one-dimensional balance. Secondly, the relative importance of pressure gradients and momentum mixing may depend on the type of model used. For instance, the LES simulations typically take advantage of their high resolution ( $O(100\text{ m})$ ) to include forcing by very high SST gradients (deSzeoeke and Bretherton, 2004; Skillingstad et al., 2007) where the advection term is likely to be large. This, together with the tendency of LES models to not represent or under-represent pressure anomalies (partly due to the small vertical extent of the domain— $O(100\text{ m})$ ), leads to a dominance of turbulent mixing effects in governing the wind speed change. In contrast, RAM models are of coarser resolution and represent fronts with widths of  $O(1/4^\circ)$ , much weaker than in LES, which forces a weaker advection term. This, combined with their good representation of pressure anomalies from the surface to above the boundary layer, may tend to give rise to the dominance of results showing pressure gradient acceleration.

The reason that many observational studies tended to discount the importance of cross-frontal pressure gradients in modifying the wind field is that most observations failed to detect a change in the pressure field in the vicinity of a front (e.g. Hashizume et al., 2002; Tokinaga et al., 2005). The perturbation pressure anomalies predicted in simulations were generally smaller than 0.1 hPa,

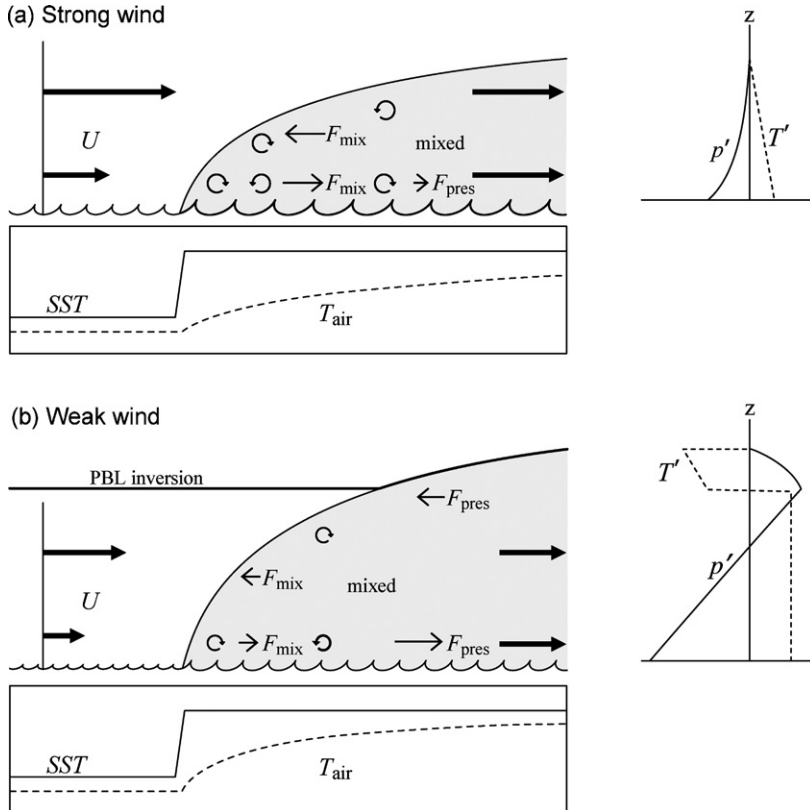


**Fig. 15.** Schematic showing boundary layer response to an ocean frontal boundary. The flow is from cold to warm SST in a situation with (a) strong background winds and (b) weak background winds. Below each panel are horizontal across-front profiles of SST and air temperature  $T_{\text{air}}$ . Above is shown the sea surface, with wave height increasing to the right of the SST front. Background winds  $U$  at left are incident on the front. A mixed internal boundary layer (gray shading) develops downstream. Circular arrows indicate the presence of turbulent eddies. Forces due to mixing ( $F_{\text{mix}}$ , term IV of Eq. (4a)) and pressure ( $F_{\text{pres}}$ , term III) are indicated with thin arrows. Due to these forces the wind profile becomes uniform with height (thick black arrows). To the right are shown vertical profiles of the downstream air temperature anomalies (dashed) and pressure anomalies (solid).

which is near the detection limit of current barometers, and much smaller than either atmospheric tides or synoptic pressure variability. However, the relatively small length scales over which these perturbation pressure anomalies act (compared to much larger scales in synoptic storms), can lead to substantial changes in the wind speed. (In fact, Cronin et al. (2003) carefully isolated the SST induced pressure signal by differencing pressure signals at two TAO moorings displaced by 200 km in the north-south direction: when the synoptic atmospheric variability is much larger than 1000 km and propagating zonally, the difference may then be attributed to local SST variations.)

### 3.3. Summary of boundary layer changes across an ocean front

Using the above descriptions of numerical and analytical model results, the main processes of boundary layer response to an ocean front are summarized in Fig. 15. This schematic shows wind flowing from cold to warm SST, under strong wind conditions (Fig. 15a), and weak winds (Fig. 15b), and is an updated and extended version of that appearing in Hsu (1984a). In this idealised scenario the role of rotation (Spall, 2007a) is not included.

In the strong wind conditions, the air temperature does not have enough time to equilibrate to SST. Further, although there are strong surface buoyancy fluxes near the surface (due to the large air-sea temperature difference), the IBL height grows slowly because of the strong advection. Meanwhile rapid changes in surface stability increase the surface roughness, and give rise to large mixing terms in the momentum budget ( $F_{\text{mix}}$  in Fig. 15) which alter the momentum balance such that momentum is transferred to the surface (Hayes et al., 1989; Spall, 2007a). In this case the resultant air temperature and pressure anomalies are small (profiles to right of schematic) and decay away from the surface as the buoyancy fluxes reduce.

In weak wind conditions, the air temperature has more time to adjust to SST. Air parcels can rise rapidly via buoyancy fluxes (less affected by horizontal advection) such that the IBL grows rapidly. In the situation shown (Fig. 15b), the IBL reaches as high as the often present inversion layer. Below the inversion layer, strong buoyancy fluxes lead to a uniform positive temperature anomaly. In contrast, due to the vertical displacement of the inversion layer, temperature anomalies above this are negative (Hashizume et al., 2002: see profile at right of Fig. 15b). In the idealized case illustrated in Fig. 15b the effect of the deeper layer of warm temperature anomalies dominates the surface pressure response which is large and negative. The resultant pressure gradient force ( $F_{\text{pres}}$ ) is to the right at the surface, and together with a reversed pressure gradient above the inversion, this acts to create a more uniform wind profile (Wai and Stage, 1989; Small et al., 2005b; Song et al., 2006). In this case, it is possible that the mixing terms close to the SST front act in a similar way to that in the strong wind case, but further downstream they are more likely to act as drag terms as the wind flows down the pressure gradient.

#### 4. Feedback from atmosphere to ocean and the fully coupled air-sea interaction

In this section the effect on the ocean of the processes discussed in Sections 2 and 3 is discussed. Firstly the effect of atmospheric boundary layer changes and consequent surface flux anomalies is considered (Section 4.1). Then, the impact of ocean surface currents on the surface stress and oceanic eddies is presented (Section 4.2). Finally the fully coupled process is introduced in Section 4.3.

##### 4.1. Feedback from atmosphere to ocean

The studies by Chelton et al. (2004), and O'Neill et al. (2005), have suggested that the atmospheric response to fine structure in the SST field may play an important role in feeding back onto the ocean, in particular through changes in the wind curl and hence Ekman pumping distribution. The Ekman pumping velocity is derived from the wind stress curl as follows:

$$w_E = \frac{1}{\rho_0} \nabla_x \frac{\tau}{f} \quad (8)$$

where  $\rho_0$  is an average water density. The modification of the sea surface height  $\eta$  of Rossby waves by Ekman pumping is then given by (White and Annis, 2003):

$$\frac{\partial \eta}{\partial t} - c_R \frac{\partial \eta}{\partial x} = - \frac{\rho'}{\rho_0} w_E + \dots \quad (9)$$

Here  $\rho'$  is the potential density difference between the upper ocean and the interior ocean, and  $c_R$  is the baroclinic Rossby wave phase speed. The corresponding sense of forced rotation in the ocean mirrors that in the atmosphere: e.g. positive (cyclonic) Ekman pumping velocity acts to decrease the sea level anomaly (SLA) thereby imparting more cyclonic vorticity to the ocean. Note that the surface stress and hence the Ekman pumping is dependent on both the atmospheric wind speed and stability, and on the ocean surface current (see (2)). The impact of the former is considered here and the latter impact is discussed in the next sub-section.

The curl and divergence anomalies associated with wind stress modifications over ocean fronts and eddies have been extensively analyzed from QuikSCAT data by Chelton et al. (2001, 2004, 2006), and O'Neill et al. (2003, 2005). A comparison of several regions based on the first year of satellite SST measurements by the AMSR-E for the 12-month period from August 2002 to July 2003 is shown in Fig. 16. The standard deviations are larger for the Kuroshio and Gulf Stream regions because of seasonal

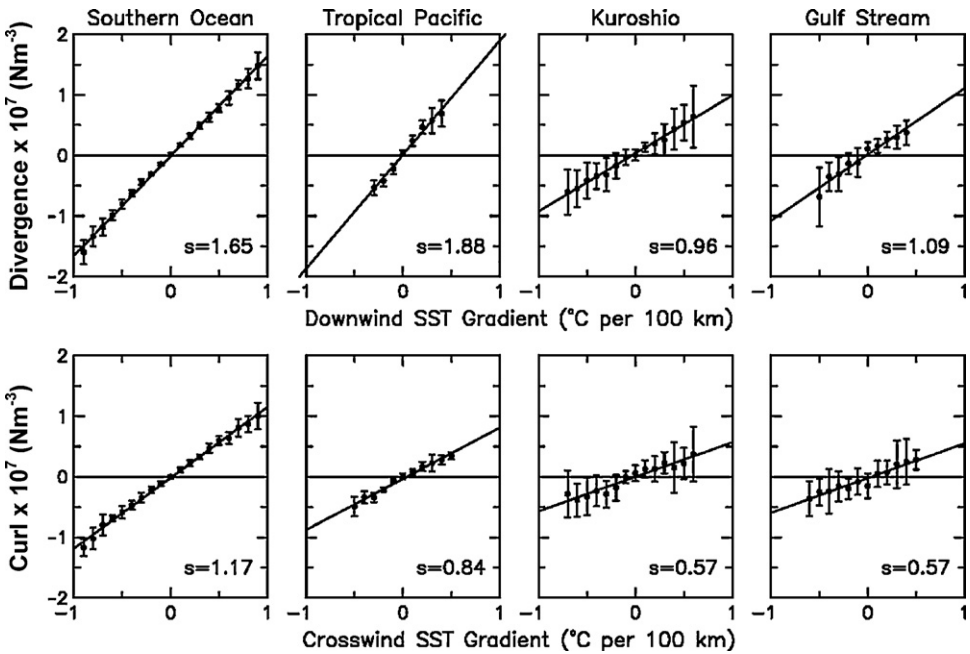


**Fig. 16.** Frontal-scale SST effects on wind stress divergence and curl. Shown are binned scatter plots of spatial high-pass filtered fields of the wind stress divergence as a function of the downwind SST gradient (top row) and the wind stress curl as a function of the crosswind SST gradient (bottom row) for four geographical regions: the Southern Ocean ( $60^{\circ}$ S to  $30^{\circ}$ S,  $0^{\circ}$  to  $360^{\circ}$ E), the eastern tropical Pacific ( $5^{\circ}$ S to  $3^{\circ}$ N,  $150^{\circ}$ W to  $100^{\circ}$ W), the Kuroshio Extension ( $32^{\circ}$ N to  $47^{\circ}$ N,  $142^{\circ}$ E to  $170^{\circ}$ W), and the Gulf Stream ( $35^{\circ}$ N to  $55^{\circ}$ N,  $60^{\circ}$ W to  $30^{\circ}$ W). The points in each panel are the means within each bin computed from 12 overlapping 6-week averages, and the error bars are the  $\pm 1$  standard deviation over the 12 samples in each bin. The wind stress divergence and curl are multiplied by  $10^7$  and the units are  $\text{Nm}^{-3}$ . From Chelton et al. (2004). Reprinted with permission from AAAS.

variations in the magnitudes of the divergence and curl perturbations. The coupling between SST and surface winds implied by the slope of the straight line fit varies geographically (and seasonally, not shown here), presumably depending on the detailed structure of the MABL, and is consistently larger for the divergence than for the curl (Chelton et al., 2004).

To give an example of their potential importance, Chelton et al. (2007a) find that the anomalies of Ekman pumping velocities due to the modification of wind stress by summertime SST mesoscale structure off the California coast had a larger dynamic range than the annual mean values.

In some cases the wind stress curl anomalies associated with ocean eddies are rectified onto the time mean state. For example, at the Equatorial Front, high values of positive wind stress curl are associated with south-easterly trade winds flowing parallel to the SST isotherms in the region between TIW cusps (Fig. 3, Chelton et al., 2001). As the trade winds are quite steady in direction, there are no compensating negative extremes of wind stress curl associated with TIWs. Hence, when a time average is made over a number of months (equivalently, several TIW periods), a narrow band of positive wind stress curl is seen, co-located with the time mean position of the Equatorial Front (Chelton et al., 2001). Kessler et al. (2003) investigated the effect of this narrow band of positive wind stress curl by computing the Sverdrup balance using time mean ERS scatterometer winds. They found that the Equatorial Undercurrent and the South Equatorial Current were much better simulated when compared to those represented by the Sverdrup balance computed using older (ship-based) wind products, that underestimate the sharp wind acceleration across the front.

Vecchi et al. (2004) also noticed wind stress curl signatures over the Great Whirl in the Arabian Sea. Noting  $1 \text{ mday}^{-1}$  Ekman pumping signals, they deduced that the  $\sim 60 \text{ m}$  thermocline displacements in the filaments and Great Whirl could be reduced by the pumping over about 1 month. Further, heat fluxes from the ocean to atmosphere could decay the SST over time scales of around 60 days. Similar

Schematic of Mesoscale Eddy in Background Westerly Wind Field

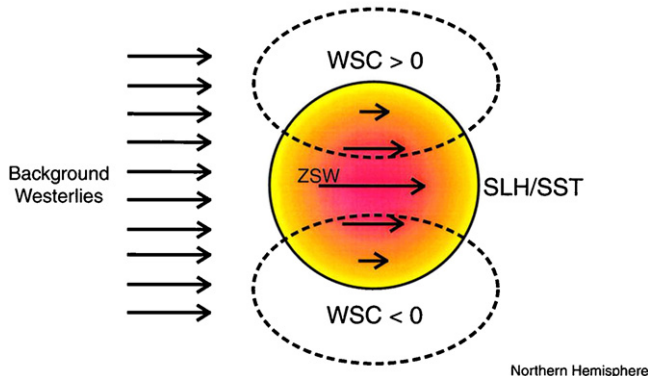


**Fig. 17.** Schematic diagram of an anti-cyclonic (warm) mesoscale eddy in a background westerly wind field, displaying the increase in scatterometer-derived (neutrally stable) zonal surface wind (ZSW) over the warm SST residual in the eddy. This yields corresponding wind stress curl (WSC) residuals, cyclonic north of the eddy and anti-cyclonic south of the eddy, which drive residual sea level height (SLH) tendencies that tend to displace the eddy toward the equator. From [White and Annis \(2003\)](#). Reproduced by permission of the American Meteorological Society.

wind modulation has been observed over transient upwelling filaments (Xie et al., 2007a) and cold wakes of typhoons over the South China Sea in summer (Lin et al., 2003). These results suggest that feedback onto the ocean is indeed an important player in the lifecycle of mesoscale ocean eddies and other transient SST features.

An idealized coupled model was employed by Chen et al. (2003) to look at the implications of air-sea coupling for oceanic frontogenesis over a continental slope. Here a primitive equation coastal ocean model was coupled to the Lindzen-Nigam (1987) MABL model. Motivated by scatterometer observations that strong winds blew parallel to the Kuroshio shelf-slope front in the East China Sea in spring, Chen et al. (2003) ran a two-dimensional across-shelf experiment initialized with a weak across-slope temperature gradient between cool shelf waters and warmer, deeper offshore water. The ensuing along front surface winds (as predicted by the Lindzen-Nigam, 1987 model) force onshore surface currents in the deep water by Ekman transport and reversed, offshore currents near the seabed. The deep water is well stratified. In contrast the shelf water is well-mixed by the wind and cools by surface latent heat loss and wind stirring, and has less cross-shelf flow. A front is formed where the two dynamical regimes meet: over the slope and coincident with high along slope winds, as observed. This example is a useful illustration of how relatively simple models can give an insight into complex phenomena, motivating more detailed studies.

White and Annis (2003: hereafter WA) studied the air-sea interaction over mesoscale eddies in background westerly flow. According to their analysis, westerly wind stress was enhanced over warm eddies and reduced over cold eddies, as measured by satellite scatterometer (as seen in Fig. 2). Further, they observed that positive sea surface height anomalies (anticyclones) were coincident with warm SST anomalies. These results were obtained by a spatial lag-correlation analysis of snapshots of the surface fields. This led them to construct the following simple model of air-sea feedback effects on eddies (see schematic reproduced in Fig. 17). Over a warm eddy in the northern hemisphere, the wind stress perturbations lead to positive wind stress curl (and Ekman pumping) north of the eddy and negative Ekman pumping to the south. This leads to a tendency to force anticyclonic circulation to the south, and cyclonic circulation to the north, of the eddy (see (9)), thus forcing the warm eddy equatorwards. (Likewise in the southern hemisphere a warm eddy would also tend equatorwards.) Note that this forcing is in addition to the forcing, discussed in Section 4.2, that arises due to the difference in wind minus ocean current from one side of the eddy to the other, referred to as the 'tophat effect' by Dewar and Flierl (1987).

Small et al. (2005a) extended the data analysis of WA to include all westward propagating mesoscale SST anomalies in the tropical belt (equatorward of 40° latitude). These anomalies are referred to here as eddies for simplicity: but note the considerable debate over whether these features are Rossby waves (Chelton and Schlaik, 1996) or closed vortices (such as those observed by Kennan and Flament, 2000, see also Chelton et al., 2007b). A cross-spectral method was applied in zonal wavenumber–frequency space to determine eddy properties from satellite data. In agreement with WA, they also found anomalies of wind stress magnitude were uniformly in phase with SST anomalies, for eddies in both westerly and easterly flow. However, different results were found concerning the relationship of eddy SST and SLA. It was found that in off-equatorial latitudes in the open ocean the anomaly of SST lead that of the SLA, consistent with the SST variability being forced by meridional eddy currents displacing mean SST fronts (which are typically, but not always, zonally aligned in the open ocean away from the western and eastern boundaries).<sup>9</sup> Near the equator, eddy SLA lead SST, consistent with meridional displacements of the Equatorial Cold Tongue front by TIWs (as the meridional SST gradient in the Equatorial Cold Tongue front is positive, the reverse of that at the higher latitude fronts). These findings are consistent with the following model.

Spall (2007b) has investigated the effect of SST induced wind stress curl anomalies on baroclinic ocean eddies using an oceanic quasi-geostrophic (QG) model with the Ekman pumping determined to be a function of the SST gradient. The numerical experiment is set up with an initial zonally aligned SST front, and a background wind flowing from south to north across the front. Using this model Spall considered the classic Eady (1949) problem of baroclinic instability of a uniform vertical shear flow. Perturbations grow along the front due to baroclinic instabilities, which propagate towards the east with a phase speed equal to half the background flow speed. Following Chelton et al. (2001) the perturbation wind stress curl is made proportional to the crosswind (zonal) temperature gradient which is set up once the instabilities grow, so that the Ekman pumping (8) is given by

$$w_E = \frac{\gamma}{\rho_0 f} \frac{\partial T}{\partial x} \quad (10)$$

where  $\gamma$  is a coupling coefficient derived from the analysis of Chelton et al. (2001). It was found that the growth rate of the instabilities could be enhanced relative to the Eady problem for uncoupled flow, when the flow is from warm to cold water. Further, the wavenumber of the fastest growing wave was found to reduce in this case. The situation may be simply visualized from Fig. 18 (reproduced from Spall, 2007b). For a background wind from the south, upwelling is forced between the cold phase of a meander of the SST front and the warm phase, following (10). The associated induced cyclonic vorticity helps to increase the amplitude of the meander, and thus the instability grows. Conversely, for background wind flow from cold to warm water, the growth rate was found to reduce and the wavenumber of the fastest growing wave increased. However, this model does not show any effect on instabilities when the background flow is along the mean front. The predictions of this analytical model agreed well with those from the primitive equation model ROMS (designed with a similar wind stress dependence on SST gradient).

Spall (2007b) found that the oceanic response is a function of the oceanic stratification, flow speed in the front, and Coriolis force, such that strong stratification, weaker jets (less advection), and low latitudes favor stronger coupling. Thus, Spall suggested that the process would be important for Tropical Instability Waves near the equator, and shelf-break fronts in summer with weak background flows, and less important for strong flows in the mid-latitude Gulf Stream and Kuroshio. It is interesting that Pezzi et al. (2004) used a similar parameterization of wind stress anomalies, and note a decrease in SST variability in TIWs when the coupling was switched on, in qualitative agreement with the theory of Spall (2007b). The decrease is likely due to the positive, meridional SST gradient at the Equatorial front, contrasting with the negative gradient at most mid-latitude fronts.

In addition to the modification of the ocean by stress effects, the heat flux anomalies which occur when the atmosphere responds to the SST gradients can also feedback onto the ocean. Large changes in

<sup>9</sup> The difference with the analysis of WA may be that their analysis focused on more isolated structures like Gulf Stream Rings, rather than meanders and instabilities which were included in the analysis of Small et al. (2005b).

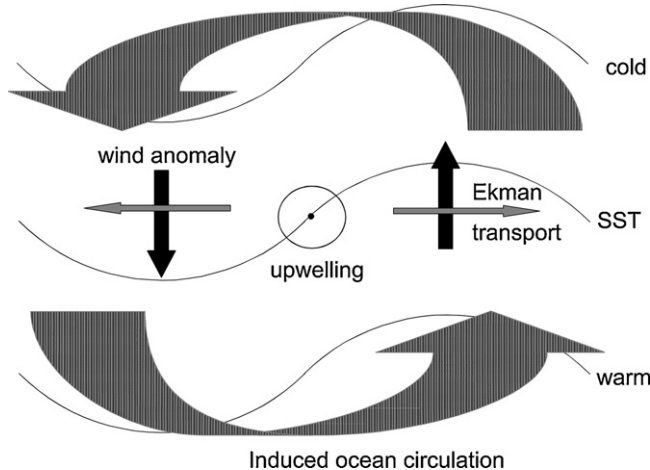


**Fig. 18.** Schematic of the ocean circulation induced by meridional background flow from south to north blowing over a front with growing meanders. Small perturbations in SST result in wind anomalies that drive divergent Ekman transport, upwelling and a cyclonic circulation anomaly. This circulation advects warm water northwards and cold water southwards, which in turn leads to larger SST anomalies and enhances the growth rate of the wave. From Spall (2007b). Reproduced by permission of the American Meteorological Society.

surface heat fluxes across fronts and eddies were documented in Section 2. Bunker and Worthington (1976) noted that large annual evaporation and sensible heat loss occurred along the Gulf Stream (displayed in Fig. 3 of Bunker and Worthington (1976), but note that the captions for their Figs. 2 and 3 appear to be erroneously swapped). Worthington (1977) hypothesized that the intense heat loss, particularly in winter when the cold north-easterly winds flow from the continent over the ocean, can lead to a significant change of Gulf Stream transport. Adamec and Elsberry (1985) suggest that the observed southward shift of the Gulf Stream in winter is due to these diabatic heat losses.

#### 4.2. Modification of coupling due to the impacts of currents on stress

The discussion in Sections 3 and 4.1 focuses on the following feedbacks: that SST impacts the atmospheric winds (via surface fluxes and induced pressure gradients) which then impact the ocean via surface stress and Ekman pumping. When considering the full ocean–atmosphere coupling another link must be added: namely that the stress is modified not just by atmospheric wind, but also by surface currents. In large-scale coupled models this has been addressed by Luo et al. (2005): here we look at some implications for air–sea interactions at smaller scales.

The surface stress is actually a function of the shear between the atmospheric wind, and the surface current. As the former is usually much greater than the latter, the latter is commonly ignored in bulk flux formulae of the surface stress (2). However, in some regions such as near the equator, where wind speeds are low and currents strong, and in western boundary current regimes, the current impact may be significant on the stress. Indeed Kelly et al. (2001), and Cornillon and Park (2001) detected equatorial ocean currents and Gulf Stream rings, respectively, in QuikSCAT scatterometer data using this method.

Dewar and Flierl (1987) considered the effect of the full formulation of stress on ocean eddies (including surface ocean current  $U_c$  in (2)) in a quasi-geostrophic framework on an  $f$  plane ( $f=f_0$ ). Linearising ( $U_{10} - U_c$ ) about the atmospheric wind, when the background wind is purely zonal, the additional Ekman pumping is approximately given by

$$w'_E \cong \frac{\rho_a}{\rho_0} C_D U_{10} \frac{2u_{cy} - v_{cx}}{f_0} \quad (11)$$

where  $U_c = (u_c, v_c)$ . This extra term results in a relaxation of the thermocline and is analogous to the bottom friction: it is referred to by Dewar and Flierl as 'top drag'. Numerical experiments showed that the dissipation of the eddy due to this top drag was over 3 times more effective than from a more standard biharmonic interior friction.

Cornillon and Park (2001) and Park et al. (2006) examined the current structure of Gulf Stream Rings through examination of components of scatterometer wind along and across the mean wind using a ring-centric coordinate system. By removing the background wind (defined as the wind averaged over an area equal to or larger than that of the Ring), they were able to estimate the ocean-current induced part of the scatterometer-measured stress, deriving current estimates that matched well with the available ADCP sections. Chelton et al. (2004) estimated the northward surface current velocity of the Gulf Stream by assuming that the zonal difference in the meridional component of stress was due to the current: the resultant estimated velocity were also very similar to previously observed current profiles.

Polito et al. (2001) computed the Ekman pumping associated with TIWs and displayed a Hovmoller diagram of the properties averaged between 1.5°N and 3.5°N. By comparing the SLA and the Ekman pumping, and finding them in phase, they deduced that the Ekman pumping was due to the surface currents of TIWs impacting on the surface stress. As suggested by Dewar and Flierl (1987), the TIW 'vortex' is feeling a drag at the sea surface.

In the study of air-sea interaction effects over ocean fronts, it would be useful to distinguish wind stress modification due to the current effect described here and modification due to the SST effect of Section 4.1. Unfortunately, in practice it can be hard to distinguish these effects in data, as most ocean fronts have both strong SST and current signatures so that the modifications can be masked. Current and future work is addressing this with coupled models such as those described in the following sub-section.

#### 4.3. The fully coupled air-sea interaction

The previous sections have discussed one-way forcing in the ocean-atmosphere system. However, it is clear from Sections 4.1 and 4.2 that a full description of air-sea interaction over fronts requires two-way modeling, such that the ocean may respond to the atmospheric changes that it induced. To study this two-way interaction, fully coupled models are required. Large-scale global coupled models have the potential to look at many oceanic fronts, but are limited in general by poor resolution in both atmosphere (where typical resolutions may be 1° or T42 horizontally, and ~20 levels in the vertical) and ocean (1° horizontally), and possibly inadequate boundary layer resolution and physical schemes.

A new approach to look at this problem is to use regional coupled models, which aim to produce more realistic simulations due to the inclusion of realistic lateral boundary conditions, higher resolution and detailed physics. By only modeling a select geographical region, these coupled models can afford high resolutions of 1/4 to 1/2°, thus enabling a detailed examination of regional processes. The simulations are constrained by lateral boundary conditions, which for the atmosphere may be given by reanalysis products or other global model data, and for the ocean may be radiation conditions or walls at ocean basin boundaries. Information can be exchanged every day or less. Typically, the ocean passes the SST to the atmospheric model, which is used in conjunction with the atmospheric variables and a bulk flux scheme to compute the air-sea fluxes, which are then passed back to ocean. (In recent modeling cases, the ocean also passes the surface current so that the surface stress can be accurately written as a function of the shear across the air-sea interface, as in Section 4.2.)

Some examples of regional coupled model studies are: Xue et al. (2000) and Li et al. (2002) analyzed the air-sea coupling in synoptic storms passing over the Gulf Stream; Perlin et al. (2007) studied how the winds and currents in the coastal upwelling zone can be influenced; Seo et al. (2007a) describe air-sea interaction over oceanic mesoscale features in the Eastern Pacific; Xie et al. (2007b) address some local processes which may affect the well-known 'tropical biases', again in the eastern Pacific; and Spall (2007a) used the Perlin et al. (2007) model for the atmospheric response studies described in Sections 3.1 and 3.2. For reference Table 3 gives more details of these models, and illustrates how the simulation time has increased recently from a few days to a few years, enabling climate time-scale issues to be addressed with these models.

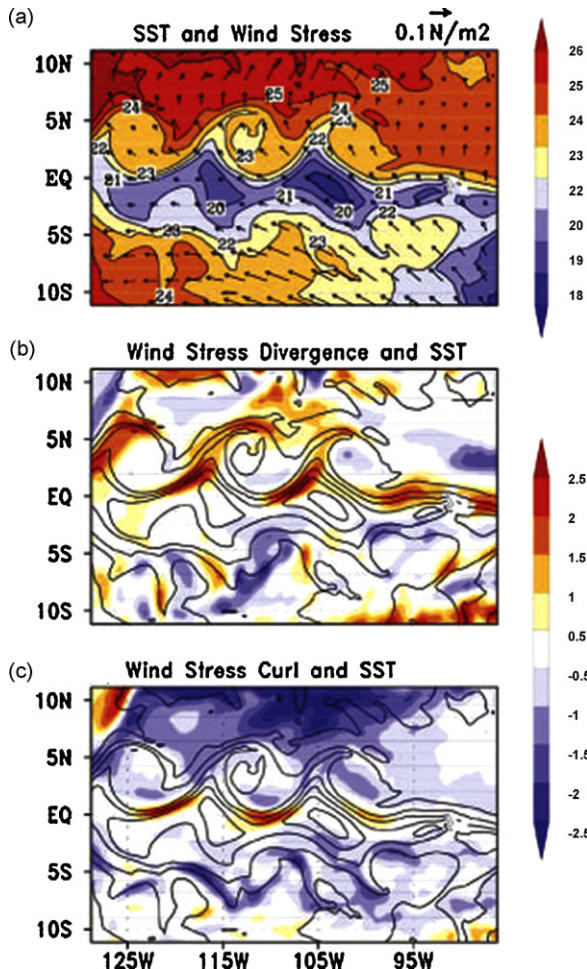


**Fig. 19.** Relationship between SST and wind stress in Tropical Instability Waves simulated by the Scripps Coupled Ocean–Atmosphere Regional Model. (a) SST ( $^{\circ}\text{C}$ , color) and wind stress vectors (see scale arrow of  $0.1 \text{ N m}^{-2}$ ), (b) wind stress divergence ( $\text{Nm}^{-2}$  per  $10^4 \text{ km}$ ) and SST ( $^{\circ}\text{C}$ , contoured), and (c) wind stress curl ( $\text{Nm}^{-2}$  per  $10^4 \text{ km}$ ) and SST ( $^{\circ}\text{C}$ , contoured). From Seo et al. (2007a). Reproduced by permission of the American Meteorological Society.

As regional coupled modeling is a newly emerging technique, their results are not described in detail here. However, as an example of their potential, we show, in Fig. 19, snapshots of the SST, wind stress, and wind stress curl and divergence over TIWs, from Seo et al. (2007a). Note that the strongest divergence is seen when the wind flows across the front, and strongest curl near the equator when it flows along the front, reproducing the observed structure around the Equatorial Front (compare with Fig. 3).

The coupled modeling study by Seo et al. (2007b) has shown that atmospheric wind response to SST anomalies in TIWs is negatively correlated with the surface currents. This indicates that TIWs are slowed down by the overlying atmospheric wind response. In an eddy kinetic energy budget analysis, they estimate this effect to be roughly 10% compared to the barotropic energy source term in the tropical Atlantic Ocean. They also showed that perturbation surface currents of TIWs can alter the surface stress estimate over the TIW region by  $\pm 20\%$ . This large alteration of surface stress by the TIW currents suggests that, in ocean models forced with QuikSCAT winds, a mismatch will occur if the model currents are not equal to the actual currents which are included in the QuikSCAT stress, leading to a possible source of error associated with this coupled feedback.

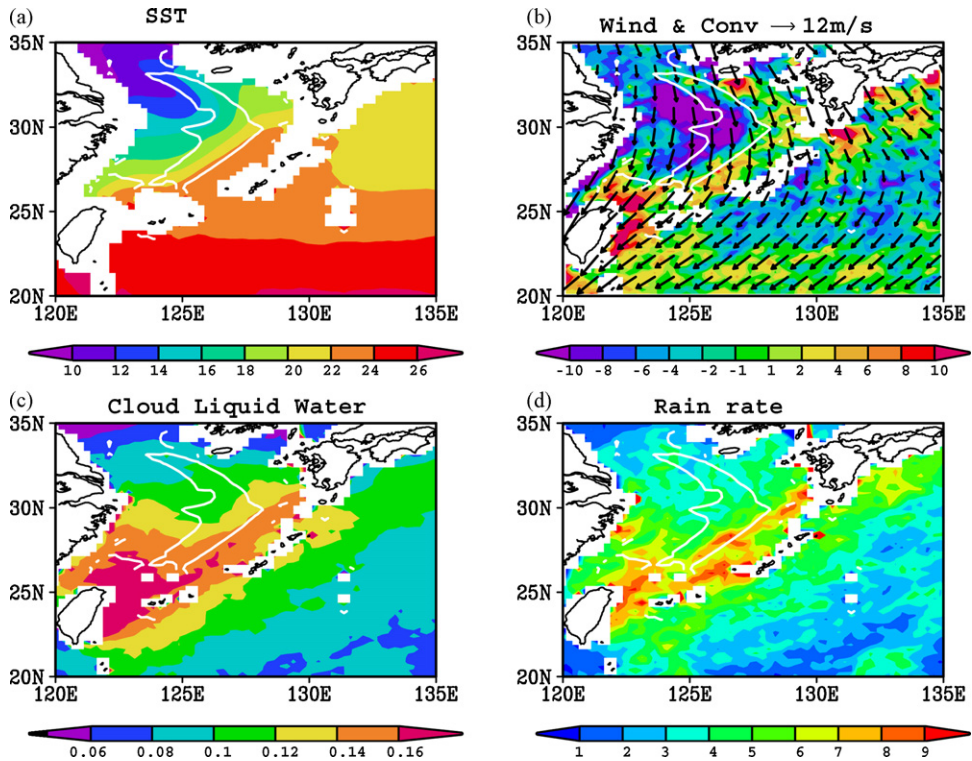


**Fig. 20.** Air-sea interaction over the Kuroshio in the east China Sea in winter. December–April averaged (a) SST ( $^{\circ}\text{C}$ , color), (b) wind-vectors ( $\text{m s}^{-1}$ , see scale arrow in title) and wind-convergence (color, multiplied by  $10^6$  with units of  $\text{s}^{-1}$ ), (c) column integrated cloud liquid water (color, mm), and (d) rain rate (color,  $\text{mm day}^{-1}$ ) observed by AMSR-E. White contours in each panel indicate SST gradient of  $3.0 \times 10^{-5} \text{ }^{\circ}\text{C m}^{-1}$ .

## 5. Discussion

The focus of this paper has been on air-sea interaction over mesoscale SST features, and its effect on the atmospheric boundary layer and the oceanic mixed layer. However, the response to the air-sea interaction is not just limited to the near-surface. In some regions of very large SST and SST gradients, observations have shown that the response can go well into the free troposphere. In situ observations of a rainband over the north wall of the Gulf Stream have been reported by Hobbs (1987) who termed it the 'Gulf Stream Rainband'. This rainband can also be associated with rapidly developing thunderstorms (Hobbs, 1987; Trunk and Bosart, 1990; Christian et al., 2003; Li et al., 2004). A rainband is also detected over the southern portion of the Kuroshio in the East China Sea in winter (Xie et al., 2002), as shown in Fig. 20. Here it is notable that the clouds are formed over the warmest water, and not over the SST gradient region. The amount of lightning associated with the Kuroshio and its Extension is less than over the Gulf Stream (Christian et al., 2003, their Fig. 4), suggesting that the atmospheric response is less deep there. Recently it has been found that in association with the rainband, the Gulf Stream anchors a maximum in climatological mean upward vertical velocity in the mid-troposphere, and upper tropospheric divergence, as shown in high resolution ECMWF operational analysis (Minobe et al., 2008). The latter can be an important forcing for stationary Rossby waves. Thus, there is a direct coupling window between the ocean and atmosphere along the Gulf Stream. Deep vertical structure in the atmospheric response to the meanders of the Agulhas Return Current in the Southern Ocean has also been detected by satellite (Liu et al., 2007).

The response of the extra-tropical atmosphere to large-scale SST anomalies has produced many varied results in global AGCMs (Kushnir et al., 2002), much of it related to the complexity of feedbacks between extra-tropical cyclones (referred to as storms here) and the mean flow. As a step towards solving this puzzle, it would be useful to understand how storms respond to smaller scale SST anomalies induced by ocean fronts and eddies. Mid-latitude storms typically grow through baroclinic instability and therefore require baroclinic sources (Chang et al., 2002). One source is the low-level (e.g. 850 h Pa to surface) temperature gradient, or baroclinicity (Hoskins and Valdes, 1990) in the atmosphere, which in turn is related to the SST gradients (Cione et al., 1993). Another source is diabatic heating which occurs when cold-air in weather systems passes over the continental coasts and over ocean SST fronts as discussed in Section 2.2. A full analysis of these effects should use new high resolution models and satellite data, current and upcoming experiments such as Kuroshio Extension System Study (Tokinaga et al., 2006), and the CLIVAR Mode Water Dynamics Experiment (CLIMODE, see [www.climode.org](http://www.climode.org)) to compliment the findings from previous studies such as GALE.

The storm response to ocean fronts has been speculated to feed back onto the ocean and create a self sustaining system. Hoskins and Valdes (1990) showed that the storm-induced diabatic heating induces a steady circulation response which includes enhanced baroclinicity in the observed storm track entrance regions of the northern hemisphere. Further, they suggest that the strong mean and variable wind stress in the storm tracks is a major component of the atmospheric forcing of warm western boundary currents, which are essential ingredients for the diabatic heating. Nakamura and Shimpo (2004) also showed that the globally strongest wind stress, found in the Southern Indian Ocean, imparted by the transient atmospheric eddies, enhances the Antarctic Circumpolar Current SST front and hence the low-level baroclinicity and the storm activity. Sampe and Xie (2007) used QuikSCAT data to show that many of the regions which exhibited high occurrence rates of very strong near-surface winds (greater than  $20 \text{ m s}^{-1}$ ) were clearly associated with the warm side of oceanic fronts. The collocation of high wind occurrence and warm meanders of major ocean fronts is a result of the combined effects of air-sea coupling over ocean fronts on the large-scale storm track distribution (as reviewed in Nakamura et al., 2004), and on the small-scale (i.e. the direct modification of the overlying winds, as reviewed in this paper).

Tropical cyclones and hurricanes can also be affected by SST gradients. As tropical cyclones require warm SST of greater than  $26^\circ\text{C}$  to fuel the latent heat release for growth (Emanuel, 2003), this is to be expected. For instance Monaldo et al. (1997: their Fig. 4) show a dramatic decrease in maximum wind of a hurricane as it crosses the Gulf Stream extension towards cooler water in mid-latitudes. Shay et al. (2000) demonstrate that not just SST, but also heat content, are important in modifying hurricanes. As features such as the loop current in the Gulf of Mexico and the Gulf Stream are associated with changes in the mixed layer depth and thus heat content, they can be important factors in hurricane intensification as suggested for the recent hurricanes of the 2004 and 2005 season (e.g. Scharroo et al., 2005).

A major feedback onto the ocean is to be expected by extra-tropical storms or tropical cyclones modified by SST gradients (or heat content gradients). Bane and Osgood (1989) note the deepening of the mixed layer by about 35 m in the Gulf Stream due to a storm which was enhanced by Gulf-Stream-modified heat fluxes. Under the extreme winds of a hurricane, mixing and evaporative effects can leave a cool wake behind it as shown by, e.g. Monaldo et al. (1997), and this may affect primary production and surface wind speed (Lin et al., 2003). This process is most effective when the mixed layer is relatively shallow, and it may have some impact on subsequent tropical cyclogenesis.

The oceanic SST fronts discussed here cause rapid changes in the atmospheric MABL over scales of a few 100s of km or much less. This has implications for atmospheric models and reanalyses which use SST as a boundary condition: the SST gradients need to be reasonably well resolved in order to get a sensible atmospheric response. For instance, Chelton (2005) has shown that the replacement of the Reynolds SST (Reynolds et al., 2002) in the ECMWF reanalysis model with that of the NOAA Real time global SST fields (RTG\_SST) on a finer grid with less smoothing, lead to an improvement in the predicted surface stress fields. These improvements in turn will lead to improved ocean circulations predicted by ocean models forced by these stress fields. Coupled climate models are starting to approach the ability of ECMWF to represent the small-scale SST/wind stress relationships (Maloney and Chelton, 2006), particularly for high resolution models such as MIROC (1.1° ocean, T106 atmosphere, Hasumi and

Emori, 2004) and the NCAR Community Climate System Model (CCSM3, 1.4° ocean, T85 atmosphere, Collins et al., 2006).

## 6. Summary

The foregoing case studies and discussions have shown that the study of air-sea interaction over fronts and eddies has progressed a long way since the early papers of Sweet et al. (1981) and Businger and Shaw (1984), aided by the advance of satellite remote sensing and numerical modeling. We can use these new results to update their description of the atmospheric MABL response, and extend it to suggest how the ocean then responds in turn as part of the fully coupled process:

- The boundary layer responds to the surface turbulent heat fluxes induced by an SST change. The heat fluxes are due to the typical sharpness of SST fronts and the slowness of the atmosphere to respond. For flow towards warm water, a well-mixed internal boundary layer can form, and the main boundary layer height and air temperature/moisture content increases. For flow towards cooler water, a shallow, stable, internal boundary layer forms with typically lower air temperature/moisture content.
- For the case of air flowing from a cold to a warm surface, turbulent mixing is enhanced within the boundary layer (or IBL) over the warm water, and momentum may be transferred to the surface, accelerating the flow there. However, for flow from warm to cold, a direct transfer of momentum appears not to be responsible for the reduction of wind speed, and the following mechanisms will be more important.
- Hydrostatic pressure anomalies are induced due to the change in air temperature and moisture induced by the SST front, with lower pressure over warm air, and higher pressure over cold air. Due to thermal advection, the length scale over which atmospheric temperature and moisture adjusts over the whole MABL may be longer than the SST frontal width. The air temperature and resulting hydrostatic pressure gradients are hence located downstream of the SST gradient.
- The change in boundary layer height will affect the surface stress, by changing the vertical scale over which stress divergence occurs. Further, the boundary layer height rise over warmer water will induce positive pressure anomalies, which tends to counteract the direct effect of near-surface warming.
- For high wind speeds and/or narrow fronts, the thermal advection is strong, and the adjustment length scales are so long that the gradients in temperature, moisture and consequently in hydrostatic pressure gradients are small. In this case changes in wind speed may be due to changes in the amount of vertical mixing as the front is crossed, and adjustments of momentum advection to the imbalance this causes in the momentum equations (see Fig. 15a).
- For low wind speeds and/or broad fronts, the thermal advection is weak, so that temperature and moisture adjust on a similar scale to the SST front (Fig. 15b). This consequently leads to a large pressure gradient which may give rise to a secondary circulation of flow across the front. This is akin to a modest sea-breeze, driven by hydrostatic pressure anomalies of the order of 0.1 hPa per °C. Because of the relatively small scales of the ocean features (compared to a synoptic atmospheric low), the pressure gradients can be enough to force velocity perturbations of  $1 \text{ m s}^{-1}$  or more.
- Away from the SST frontal zone, surface stress is found to be positively correlated with SST. There are a number of contributing factors to this: (i) the drag coefficient increases under more unstable conditions (ii) the wind above the surface is stronger under unstable conditions (iii) under equilibrium conditions the change in boundary layer height modifies the stress. Most studies have found that the first effect is small.
- As a consequence of the increased stress over warmer water, wind stress curl is related to the component of background wind along the SST front, whilst wind stress divergence is related to the component across the front. These relationships have been found to be close to linear for most eddy-active regions of the globe.
- The consequent Ekman pumping anomaly modifies ocean currents and circulation. Near the Equator a band of narrow wind stress curl in the time mean affects equatorial currents. For closed eddies such as Gulf Stream Rings, the induced wind stress curl anomaly under mean westerly winds may

enforce a southward migration of the eddies. For more wavelike ocean features such as meanders along mid-latitude SST fronts, the Ekman pumping may act to enhance the SST variability in some circumstances, reduce in others, or have no effect, depending on the background wind direction.

- Ekman pumping is also modified by ocean currents dragging against the wind at the air-sea interface. The consequence is a dissipation of ocean eddies.
- Atmospheric response is not just confined to the boundary layer, as indicated by the Gulf Stream rainband with accompanying lightning strikes and upper tropospheric divergence anomalies. Synoptic storms are also modified by the SST gradients associated with western boundary current systems. This suggests that interannual and decadal variability of ocean currents systems may impact the atmospheric variability and climate.

Although much progress has been made in this topic, it is clear that much also remains unclear. For instance, the study of the response of the ocean to small-scale Ekman pumping anomalies, and the fully coupled air-sea response, is still in preliminary stages. Such questions as: does the ocean respond deeper than the mixed layer, does the atmospheric storm track move in response to variations in ocean frontal location over long time scales, and does the atmospheric response to transient eddies rectify into interannual variability (Seo et al., 2006; Jochum et al., 2007) are still a matter of much debate.

Numerical models will play an important role in the future in resolving these issues. Especially with the steady increase in computer power and storage, and increasingly sophisticated numerical algorithms, it is now possible to run global atmospheric models at T1279 resolution (with about a 10 km grid, Ohfuchi et al., 2005), multi-decade ocean models at 0.1° (Sasaki and Nonaka, 2006; Taguchi et al., 2007), and century long simulation ocean-atmosphere climate models at resolutions of T106 (~1.125°) for the atmosphere and 0.2–0.3° for the ocean (Hasumi and Emori, 2004). At these resolutions they can take maximum advantage of data assimilation of high resolution satellite data. The improved resolution of ocean fronts and their accompanying air-sea interaction processes may enhance model nowcasts and forecasts, as shown by Chelton (2005) for the ECMWF model. Together with continued field experiments to understand the fundamental boundary layer physical processes that lead to improved algorithms, these techniques promise to rapidly enhance our understanding of the role of ocean fronts and eddies on climate variability.

## Acknowledgements

Our thanks go to Dudley Chelton and Roger Samelson for reading an early version of the manuscript and for making very valuable suggestions and contacts. Igor Belkin's suggestion to write the review paper motivated this very enjoyable piece of work. Markus Jochum and 4 anonymous reviewers provided detailed and helpful comments which helped improve the paper. Steve Businger helpfully provided insight on synoptic storm response. Chris Fairall and Albert Romero gave support and artwork assistance for Fig. 15. Jan Hafner prepared Fig. 1. S.-P.X. and R.J.S. were supported by NASA (grant NAG-10045 and JPL contract 1216010), NOAA (NA17RJ1230), NSF (ATM01-04468 and ATM00-02322), and by the Japan Agency for Marine-Earth Science and Technology (JAMSTEC) through its sponsorship of the International Pacific Research Center. M.S. was supported by ONR grant N00014-05-1-0300. H.S. was supported by the NOAA Climate and Global Change Postdoctoral Fellowship Program, administered by the University Corporation for Atmospheric Research. L.O.N. was supported by NASA (Grant NAS5-32965 Contract 1283973) and the National Research Council Postdoctoral Research Associateship Award. Q.S. was supported by NASA (grant NAS5-32965) via Oregon State University. Support for P.C. was provided by the State of Rhode Island and Providence Plantations. IPRC contribution number 535 and SOEST contribution number 7505.

## References

- Adamec, D., Elsberry, R.L., 1985. The response of intense oceanic current systems entering regions of strong cooling. *J. Phys. Oceanogr.* 15, 1284–1295.
- Anderson, S.P., 2001. On the atmospheric boundary layer over the equatorial front. *J. Climate* 14, 1688–1695.
- Bane, J.M., Osgood, K.E., 1989. Wintertime air-sea interaction processes across the Gulf Stream. *J. Geophys. Res.* 94, 10755–10772.

- Battisti, D.S., Sarachik, E.S., Hirst, A.C., 1999. A consistent model for the large scale steady surface atmospheric circulation in the Tropics. *J. Climate* 12, 2956–2964.
- Beal, R.C., Kudryavtsev, V.N., Thompson, D.R., Grodsky, S.A., Tilley, D.C., Dulov, V.A., Gruber, H.C., 1997. The influence of the marine atmospheric boundary layer on ERS 1 synthetic aperture radar imagery of the Gulf Stream. *J. Geophys. Res.* 102, 5799–5814.
- Belkin, I.M., Romanov, Y.A., 1990. Surface currents and temperature fronts of the southern Indian Ocean. *Oceanology (English Translation)* 30, 25–28.
- Blumberg, A.F., Mellor, G.L., 1987. A description of a three-dimensional coastal ocean circulation model. In: Heaps, N.S. (Ed.), *Three-dimensional Coastal Ocean Models*, vol. 4. Amer. Geophys. Union, pp. 1–16.
- Boebel, O., Lutjeharms, J.R.E., Schmid, C., Zenk, W., Rossby, T., Barron, C., 2003b. The Cape Cauldron: a regime of turbulent inter-ocean exchange. *Deep-Sea Res. II* 50, 57–86.
- Boebel, O., Rossby, T., Lutjeharms, J., Zenk, W., Barron, C., 2003a. Path and variability of the Agulhas return current. *Deep-Sea Res. II* 50, 35–56.
- Bourras, D., Reverdin, G., Giordani, H., Caniaux, G., 2004. Response of the atmospheric boundary layer to a mesoscale oceanic eddy in the northeast Atlantic. *J. Geophys. Res.* 109, D18114, doi:10.1029/2004JD004799.
- Brown, R.A., 1982. On two-layer models and the similarity functions for the PBL. *Bound.-Layer Meteor.* 24, 451–463.
- Brown, R.A., Liu, W.T., 1982. An operational large-scale marine planetary boundary layer model. *J. Appl. Meteor.* 21, 261–269.
- Bunker, A.F., Worthington, L.V., 1976. Energy exchange charts of the North Atlantic Ocean. *Bull. Am. Meteor. Soc.* 57, 670–678.
- Businger, J.A., Shaw, W.J., 1984. The response of the marine boundary layer to mesoscale variations in sea-surface temperature. *Dyn. Atmos. Oceans* 8, 267–281.
- Businger, S., Graziano, T.M., Kaplan, M.L., Rozumalski, R.A., 2005. Cold-air cyclogenesis along the Gulf Stream front: investigation of diabatic impacts on cyclone development, frontal structure and track. *Meteor. Atmos. Phys.* 88, 65–90.
- Carson, R.B., 1950. The Gulf Stream Front: a cause of stratus on the lower Atlantic coast. *Mon. Wea. Rev.* 78, 91–101.
- Chang, E.K.M., Lee, S., Swanson, K.L., 2002. Storm track dynamics. *J. Climate* 15, 2163–2183.
- Chelton, D.B., 2005. The impact of SST specification on ECMWF surface wind stress fields in the Eastern Tropical Pacific. *J. Climate* 18, 530–550.
- Chelton, D.B., deSzoeke, R.A., Schlax, M.G., El Naggar, K., Siwertz, N., 1998. Geographical variability of the first baroclinic Rossby radius of deformation. *J. Phys. Oceanogr.* 28, 433–460.
- Chelton, D.B., Esbensen, S.K., Schlax, M.G., Thum, N., Freilich, M.H., Wentz, F.J., Gentemann, C.L., McPhaden, M.J., Schopf, P.S., 2001. Observations of coupling between surface wind stress and sea surface temperature in the Eastern Tropical Pacific. *J. Climate* 14, 1479–1498.
- Chelton, D.B., Freilich, M.H., Sienkiewicz, J.M., Von Ahn, J.M., 2006. On the use of QuikSCAT scatterometer measurements of surface winds for marine weather predictions. *Mon. Wea. Rev.* 134, 2055–2071.
- Chelton, D.B., Schlax, M.G., 1996. Global observations of oceanic Rossby waves. *Science* 272, 234–238.
- Chelton, D.B., Schlax, M.G., Freilich, M.H., Milliff, R.F., 2004. Satellite measurements reveal persistent small-scale features in ocean winds. *Science* 303, 978–983.
- Chelton, D.B., Schlax, M.G., Samelson, R.M., 2007a. Summertime coupling between sea surface temperature and wind stress in the California Current System. *J. Phys. Oceanogr.* 37, 495–517.
- Chelton, D.B., Schlax, M.G., Samelson, R.M., deSzoeke, R.A., 2007b. Global observations of large oceanic eddies. *Geophys. Res. Lett.* 34, L15606, doi:10.1029/2007GL030812.
- Chen, D., Liu, W.T., Tang, W., Wang, Z., 2003. Air-sea interaction at an oceanic front: Implications for frontogenesis and primary production. *Geophys. Res. Lett.* 30, 1745, doi:10.1029/2003GL017536.
- Christian, H.J., Blakeslee, R.J., Boccippio, D.J., Boeck, W.L., Buechler, D.E., Driscoll, K.T., Goodman, S.J., Hall, J.M., Koshak, W.J., Mach, D.M., Stewart, M.F., 2003. Global frequency and distribution of lightning as observed from space by the Optical Transient Detector. *J. Geophys. Res.* 108, 4005, doi:10.1029/2002JD002347.
- Cione, J.J., Raman, S., Pietrafesa, L.J., 1993. The effect of Gulf Stream-induced baroclinicity on U.S. East Coast winter cyclones. *Mon. Wea. Rev.* 121, 421–430.
- Collins, W.D., Bitz, C.M., Blackmon, M.L., Bonan, G.B., Bretherton, C.S., Carton, J.A., Chang, P., Doney, S.C., Hack, J.J., Henderson, T.B., Kiehl, J.T., Large, W.G., McKenna, D.S., Santer, B.D., Smith, R.D., 2006. The community climate system model version 3 (CCSM3). *J. Climate* 19, 2122–2143.
- Colucci, S.J., 1976. Winter cyclone frequencies over the eastern United States and adjacent western Atlantic, 1964–1973. *Bull. Am. Meteor. Soc.* 57, 548–553.
- Cornillon, P., Park, K.-A., 2001. Warm core ring velocities inferred from NSCAT. *Geophys. Res. Lett.* 28, 575–578.
- Cronin, M.F., Xie, S.-P., Hashizume, H., 2003. Barometric pressure variations associated with Eastern Pacific Tropical Instability Waves. *J. Climate* 16, 3050–3057.
- Deser, C., Bates, J.J., Wahl, S., 1993. The influence of sea surface temperature gradients on stratiform cloudiness along the Equatorial Front in the Pacific Ocean. *J. Climate* 6, 1172–1180.
- deSzoeke, S.P., Bretherton, C.S., 2004. Quasi-Lagrangian large eddy simulations of cross-equatorial flow in the east Pacific atmospheric boundary layer. *J. Atmos. Sci.* 61, 1837–1858.
- deSzoeke, S.P., Bretherton, C.S., Bond, N.A., Cronin, M.F., Morley, B.M., 2005. EPIC 95°W Observations of the Eastern Pacific atmospheric boundary layer from the cold tongue to the ITCZ. *J. Atmos. Sci.* 62, 426–442.
- Dewar, W.K., Flierl, G.R., 1987. Some effects of the wind on rings. *J. Phys. Oceanogr.* 17, 1653–1667.
- Dirks, R.A., Kuettner, J.P., Moore, J.A., 1988. Genesis of Atlantic Lows Experiment (GALE): an overview. *Bull. Am. Meteor. Soc.* 69, 148–160.
- Doyle, J.D., Warner, T.T., 1990. Mesoscale coastal processes during GALE IOP 2. *Mon. Wea. Rev.* 118, 283–308.
- Doyle, J.D., Warner, T.T., 1993. The impact of the sea surface temperature resolution on mesoscale coastal processes during GALE IOP2. *Mon. Wea. Rev.* 121, 313–334.
- Driedonks, A.G.M., 1982. Sensitivity analysis of the equations for a convective mixed layer. *Bound.-Layer Meteor.* 22, 475–480.
- Düing, W., Hisard, P., Katz, E., Meincke, J., Miller, L., Moroshkin, K.V., Philander, G., Ribnikov, A.A., Voigt, K., Weisberg, R., 1975. Meanders and long waves in the equatorial Atlantic. *Nature* 257, 280–284.
- Eady, E.T., 1949. Long waves and cyclone waves. *Tellus* 1, 33–52.

- Emanuel, K., 2003. Tropical cyclones. *Ann. Rev. Earth Planet. Sci.* 31, 75–104.
- Eymard, L., 1998. Introduction: the SEMAPHORE experiment. *J. Geophys. Res.* 103, 25005–25008.
- Fairall, C.W., Bradley, E.F., Rogers, D.P., Edson, J.B., Young, G.S., 1996. Bulk parameterization of air-sea fluxes for Tropical Ocean–Global Atmosphere Coupled–Ocean Atmosphere Response Experiment. *J. Geophys. Res.* 101, 3747–3764.
- Friehe, C.A., Shaw, W.J., Rogers, D.P., Davidson, K.L., Large, W.G., Stage, S.A., Crescenti, G.H., Khalsa, S.J.S., Greenhut, G.K., Li, F., 1991. Air–sea fluxes and surface layer turbulence around a sea-surface temperature front. *J. Geophys. Res.* 96, 8593–8609.
- Gamo, M., Yamamoto, S., Yokoyama, O., Yoshikado, H., 1983. Structure of the free convective internal boundary-layer above the coastal area. *J. Meteor. Soc. Jpn.* 61, 110–124.
- Gill, A.E., 1980. Some simple solutions for heat-induced tropical circulation. *Quart. J. R. Meteor. Soc.* 106, 447–462.
- Gill, A.E., Rasmusson, E.M., 1983. The 1982–83 climate anomaly in the equatorial Pacific. *Nature* 306, 229–234.
- Giordani, H., Planton, S., Bénech, B., Kwon, B.-H., 1998. Atmospheric boundary layer response to sea surface temperatures during the SEMAPHORE experiment. *J. Geophys. Res.* 103, 25047–25060.
- Hadley, G., 1735. Concerning the cause of the general trade-winds. *Philos. Trans.* 39, 58–62.
- Halley, E., 1686. An historical account of the trade winds, and monsoons, observable in the seas between and near the tropicks, with an attempt to assign the physical cause of the said winds. *Philos. Trans.* 16, 153–168.
- Hashizume, H., Xie, S.-P., Fujiwara, M., Shiotani, M., Watanabe, T., Tanimoto, Y., Liu, W.T., Takeuchi, K., 2002. Direct observations of atmospheric boundary layer response to SST variations associated with tropical instability waves over the eastern equatorial Pacific. *J. Climate* 15, 3379–3393.
- Hashizume, H., Xie, S.-P., Liu, W.T., Takeuchi, K., 2001. Local and remote response to tropical instability waves: a global view from space. *J. Geophys. Res.* 106, 10173–10185.
- Hasumi, H., Emori, S. (Eds.), 31 coauthors, 2004. K-1 coupled GCM (MIROC) description. K-1 Technical Report No. 1. Center for Climate System Research, University of Tokyo, NIES, FRCGC, Japan. WWW page: <http://www.ccsr.u-tokyo.ac.jp/kyosei/hasumi/MIROC/tech-repo.pdf>.
- Hayes, S.P., McPhaden, M.J., Wallace, J.M., 1989. The influence of sea surface temperature on surface wind in the eastern equatorial Pacific: weekly to monthly variability. *J. Climate* 2, 1500–1506.
- Hirst, A.C., 1986. Unstable and damped equatorial modes in simple coupled ocean–atmosphere models. *J. Atmos. Sci.* 43, 606–630.
- Hobbs, P.V., 1987. The Gulf-Stream Rainband. *Geophys. Res. Lett.* 14, 1142–1145.
- Hodur, R.M., 1997. The Naval Research Laboratory's Coupled Ocean/Atmosphere Mesoscale Prediction System (COAMPS). *Mon. Wea. Rev.* 125, 1414–1430.
- Holt, T.R., Raman, S., 1992. Three-dimensional mean and turbulence structure of a coastal front influenced by the Gulf Stream. *Mon. Wea. Rev.* 120, 17–39.
- Holton, J.R., 2004. An Introduction to Dynamical Meteorology, fourth edition. Elsevier Academic Press, London, 535 pp.
- Hong, S.Y., Pan, H.L., 1996. Nonlocal boundary layer vertical diffusion in a medium-range forecast model. *Mon. Wea. Rev.* 124, 2322–2338.
- Hoskins, B.J., McIntyre, M.E., Robertson, A.W., 1985. On the use and significance of isentropic potential vorticity maps. *Quart. J. R. Meteor. Soc.* 111, 877–946.
- Hoskins, B.J., Valdes, P.J., 1990. On the existence of storm tracks. *J. Atmos. Sci.* 47, 1854–1864.
- Hsu, S.A., 1984a. Effect of cold-air advection on internal boundary-layer development over warm oceanic currents. *Dyn. Atmos. Ocean* 8, 307–319.
- Hsu, S.A., 1984b. Sea-breeze-like winds across the north wall of the Gulf-Stream: an analytical model. *J. Geophys. Res.* 89, 2025–2028.
- Huang, C.-Y., Raman, S., 1988. A numerical modeling study of the marine boundary layer over the Gulf Stream during cold air advection. *Bound.-Layer Meteor.* 45, 251–290.
- Jochum, M., Deser, C., Phillips, A., 2007. Tropical atmospheric variability forced by oceanic internal variability. *J. Climate* 20, 765–771.
- Juang, H.-M.H., Hong, S.-Y., Kanamitsu, M., 1997. The NCEP regional spectral model: an update. *Bull. Am. Meteor. Soc.* 78, 2125–2143.
- Jury, M.R., 1994. A thermal front within the marine atmospheric boundary-layer over the Agulhas Current south of Africa: composite aircraft observations. *J. Geophys. Res.* 99, 3297–3304.
- Jury, M.R., Walker, N., 1988. Marine boundary layer modification across the edge of the Agulhas Current. *J. Geophys. Res.* 93, 647–654.
- Kelly, K.A., Dickinson, S., McPhaden, M.J., Johnson, G.C., 2001. Ocean currents evident in satellite wind data. *Geophys. Res. Lett.* 28, 2469–2472.
- Kennan, S.C., Flament, P.J., 2000. Observations of a tropical instability vortex. *J. Phys. Oceanogr.* 30, 2277–2301.
- Kessler, W.S., Johnson, G.C., Moore, D.W., 2003. Sverdrup and nonlinear dynamics of the Pacific Equatorial currents. *J. Phys. Oceanogr.* 33, 994–1008.
- Khalsa, S.J.S., Greenhut, G.K., 1989. Atmospheric turbulence structure in the vicinity of an oceanic front. *J. Geophys. Res.* 94, 4913–4922.
- Killworth, P.D., Chelton, D.B., deSzoeke, R.A., 1997. The speed of observed and theoretical long extratropical planetary waves. *J. Phys. Oceanogr.* 27, 1946–1966.
- Koračin, D., Rogers, D.P., 1990. Numerical simulations of the response of the marine atmosphere to ocean forcing. *J. Atmos. Sci.* 47, 592–611.
- Kuo, Y.-H., Reed, R.J., Low-Nam, S., 1991. Effects of surface energy fluxes during the early development and rapid intensification stages of seven explosive cyclones in the western Atlantic. *Mon. Wea. Rev.* 119, 457–475.
- Kushnir, Y., Robinson, W.A., Bladé, I., Hall, N.M.J., Peng, S., Sutton, R., 2002. Atmospheric GCM response to extratropical SST anomalies: synthesis and evaluation. *J. Climate* 15, 2233–2256.
- Kwon, B.-H., Bénech, B., Lambert, D., Durand, P., Druihet, A., Giordani, H., Planton, S., 1998. Structure of the marine atmospheric boundary layer over an oceanic thermal front: SEMAPHORE experiment. *J. Geophys. Res.* 103, 25159–25180.
- Lee-Thorp, A.M., Rouault, M., Lutjeharms, J.R.E., 1998. Cumulus cloud formation above the Agulhas current. *S. Afr. J. Sci.* 94, 351–354.

- Legeckis, R., 1977. Long waves in the eastern equatorial Pacific Ocean: a view from a geostationary satellite. *Science* 197, 1179–1181.
- Li, X., Zheng, W., Pichel, W.G., Zou, C.-Z., Clemente-Colón, P., Friedman, K.S., 2004. A cloud line over the Gulf Stream. *Geophys. Res. Lett.* 31, L14108, doi:10.1029/2004GL019892.
- Li, Y., Xue, H., Bane, J.M., 2002. Air-sea interactions during the passage of a winter storm over the Gulf Stream: a three-dimensional coupled atmosphere-ocean model study. *J. Geophys. Res.* 107, 3200, doi:10.1029/2001JC001161.
- Lin, I., Liu, W.T., Wu, C.-C., Wong, G.T.F., Hu, C., Chen, Z., Liang, W.-D., Yang, Y., Liu, K.-K., 2003. New evidence for enhanced ocean primary production triggered by tropical cyclone. *Geophys. Res. Lett.* 30, 1718, doi:10.1029/2003GL017141.
- Lindzen, R.S., Nigam, S., 1987. On the role of sea surface temperature gradients in forcing low level winds and convergence in the tropics. *J. Atmos. Sci.* 44, 2418–2436.
- Liu, W.T., Katsaros, K.B., Businger, J.A., 1979. Bulk parameterization of air-sea exchanges of heat and water vapor including the molecular constraints at the interface. *J. Atmos. Sci.* 36, 1722–1735.
- Liu, W.T., Xie, X., Niiler, P.P., 2007. Ocean-atmosphere interaction over Agulhas extension meanders. *J. Climate* 20, 5784–5797.
- Liu, W.T., Xie, X., Polito, P.S., Xie, S.-P., Hashizume, H., 2000. Atmospheric manifestation of tropical instability wave observed by QuikSCAT and tropical rain measuring mission. *Geophys. Res. Lett.* 27, 2545–2548.
- Liu, W.T., Zhang, A., Bishop, J.K.B., 1994. Evaporation and solar irradiance as regulators of sea surface temperature in annual and interannual changes. *J. Geophys. Res.* 99, 12623–12637.
- Luo, J.-J., Masson, S., Roeckner, E., Madec, G., Yamagata, T., 2005. Reducing climatology bias in an ocean-atmosphere CGCM with improved coupling physics. *J. Climate* 18, 2344–2360.
- Lutjeharms, J.R.E., Mey, R.D., Hunter, I.E., 1986. Cloud lines over the Agulhas current. *S. Afr. J. Sci.* 82, 635–640.
- Lutjeharms, J.R.E., Rouault, M., 2000. Observations of cloud formation above Agulhas current intrusions in the southeast Atlantic. *S. Afr. J. Sci.* 96, 577–580.
- Lutjeharms, J.R.E., van Balleidooyen, R.C., 1984. Topographic control in the Agulhas current system. *Deep-Sea Res.* 31, 1321–1337.
- Lyman, J.M., Johnson, G.C., Kessler, W.S., 2007. Distinct 17 day and 33 day tropical instability waves in subsurface observations. *J. Phys. Oceanogr.* 37, 855–872.
- McCauley, M., Zhang, C., Bond, N.A., 2004. Large-scale characteristics of the atmospheric boundary layer in the Eastern Pacific Cold Tongue-ITCZ region. *J. Climate* 17, 3907–3920.
- Maloney, E.D., Chelton, D.B., 2006. An assessment of the sea surface temperature influence on surface wind stress in numerical weather prediction and climate models. *J. Climate* 19, 2743–2762.
- Mantua, N.J., Hare, S.R., Zhang, Y., Wallace, J.M., Francis, R.C., 1997. A Pacific interdecadal climate oscillation with impacts on salmon production. *Bull. Am. Meteor. Soc.* 78, 1069–1079.
- Mey, R.D., Walker, N.D., Jury, M.R., 1990. Surface heat fluxes and marine boundary layer modification in the Agulhas Retroflection region. *J. Geophys. Res.* 95, 15997–16015.
- Minobe, S., Kuroano-Yoshida, A., Komori, N., Xie, S.-P., Small, R.J., 2008. Influence of the Gulf Stream on the troposphere. *Nature* 452, 206–209, doi:10.1038/nature06690.
- Mitchell, T.P., Wallace, J.M., 1992. The annual cycle in Equatorial convection and sea surface temperature. *J. Climate* 5, 1140–1155.
- Monaldo, F.M., Sikora, T.D., Babin, S.M., Sternier, R.E., 1997. Satellite imagery of sea surface temperature cooling in the wake of Hurricane Edouard (1996). *Mon. Wea. Rev.* 125, 2716–2721.
- Nakamura, H., Sampe, T., Tanimoto, Y., Shimpo, A., 2004. Observed associations among storm tracks, jet streams, and midlatitude oceanic fronts. *AGU Geophys. Monogr. Ser.* 147, 329–346.
- Nakamura, H., Shimpo, A., 2004. Seasonal variations in the Southern hemisphere storm tracks and jet streams as revealed in a reanalysis dataset. *J. Climate* 17, 1828–1844.
- Neelin, J.D., 1989. On the interpretation of the Gill model. *J. Atmos. Sci.* 46, 2466–2468.
- Neiman, P.J., Shapiro, M.A., 1993. The life cycle of an extratropical marine cyclone. Part 1: Frontal-cyclone evolution and thermodynamic air-sea interaction. *Mon. Wea. Rev.* 121, 2153–2176.
- Nonaka, M., Xie, S.-P., 2003. Covariations of sea surface temperature and wind over the Kuroshio and its extension: evidence for ocean-to-atmosphere feedback. *J. Climate* 16, 1404–1413.
- Ohfuchi, W., Sasaki, H., Masumoto, Y., Nakamura, H., 2005. Mesoscale resolving simulations of the global atmosphere and ocean on the earth simulator. *EOS Trans. Am. Geophys. Union* 86, 45–46.
- Okumura, Y., Xie, S.-P., Numaguti, A., Tanimoto, Y., 2001. Tropical Atlantic air-sea interaction and its influence on the NAO. *Geophys. Res. Lett.* 28, 1507–1510.
- O'Neill, L.W., Chelton, D.B., Esbensen, S.K., 2003. Observations of SST-induced perturbations of the wind stress field over the Southern Ocean on seasonal time scales. *J. Climate* 16, 2340–2354.
- O'Neill, L.W., Chelton, D.B., Esbensen, S.K., Wentz, F.J., 2005. High-resolution satellite measurements of the atmospheric boundary layer response to SST variations along the Agulhas Return Current. *J. Climate* 18, 2706–2723.
- Pacanowski, R.C., Griffies, S.M., 2000. The MOM3 Manual. GFDL Ocean Group Tech. Rep. 4. Geophysical Fluid Dynamics Laboratory, Princeton, NJ. 680 pp. WWW page: <http://www.gfdl.noaa.gov/~smg/MOM/web/guide.parent/guide.parent.html>.
- Park, K.-A., Cornillon, P.C., 2002. Stability-induced modification of sea surface winds over Gulf Stream rings. *Geophys. Res. Lett.* 29, 2211, doi:10.1029/2001GL014236.
- Park, K.-A., Cornillon, P.C., Codiga, D.L., 2006. Modification of surface winds near ocean fronts: effects of Gulf Stream rings on scatterometer (QuikSCAT, NSCAT) wind observations. *J. Geophys. Res.* 111, C03021, doi:10.1029/2005JC003016.
- Pazan, S.E., Niiler, P., 2004. New global drifter data set available. *EOS, Trans. Am. Geophys. Union* 85, 17, doi:10.1029/2004EO020007.
- Perlin, N., Skillingstad, E.D., Samelson, R.M., Barbour, P.L., 2007. Numerical simulation of air-sea coupling during coastal upwelling. *J. Phys. Oceanogr.* 37, 2081–2093.
- Pezzi, L.P., Vialard, J., Richards, K.J., Menkes, C., Anderson, D., 2004. Influence of ocean-atmosphere coupling on the properties of tropical instability waves. *Geophys. Res. Lett.* 31, L16306, doi:10.1029/2004GL019995.
- Philander, S.G.H., Yamagata, T., Pacanowski, R.C., 1984. Unstable air-sea interactions in the tropics. *J. Atmos. Sci.* 41, 604–613.
- Polito, P.S., Ryan, J.P., Liu, W.T., Chavez, F.P., 2001. Oceanic and atmospheric anomalies of tropical instability waves. *Geophys. Res. Lett.* 28, 2233–2236.

- Raymond, D.J., Esbensen, S.K., Paulson, C., Gregg, M., Bretherton, C.S., Peterson, W.A., Cifelli, R., Shay, L.K., Ohlmann, C., Zuidema, P., 2004. EPIC2001 and the coupled ocean–atmosphere system of the tropical east Pacific. *Bull. Am. Meteor. Soc.* 85, 1341–1354.
- Reason, C.J.C., 2001. Evidence for the influence of the Agulhas Current on regional atmospheric circulation patterns. *J. Climate* 14, 2769–2778.
- Reed, R.J., Stoebring, M.T., Kuo, Y.-H., 1992. A model-aided study of the origin and evolution of the anomalously high potential vorticity in the inner region of a rapidly deepening marine cyclone. *Mon. Wea. Rev.* 120, 893–913.
- Reynolds, R.W., Rayner, N.A., Smith, T.M., Stokes, D.C., Wang, W., 2002. An improved in situ and satellite SST analysis for climate. *J. Climate* 15, 1609–1625.
- Riordan, A.J., Lin, Y.-L., 1992. Mesoscale wind signatures along the Carolina Coast. *Mon. Wea. Rev.* 120, 2786–2797.
- Rogers, D.P., 1989. The marine boundary layer in the vicinity of an ocean front. *J. Atmos. Sci.* 46, 2044–2062.
- Rouault, M., Lee-Thorp, A.M., 1996. Fine-time resolution measurements of atmospheric boundary layer properties between Cape Town and Marion Island. *S. Afr. J. Mar. Sci.* 17, 281–296.
- Rouault, M., Lee-Thorp, A.M., Lutjeharms, J.R.E., 2000. The atmospheric boundary layer above the Agulhas Current during alongcurrent winds. *J. Phys. Oceanogr.* 30, 40–50.
- Rouault, M., Lutjeharms, J.R.E., 2000. Air-sea exchange over an Agulhas eddy at the subtropical convergence. *Global Atmos. Ocean Syst.* 7, 125–150.
- Rouault, M., Reason, C.J.C., Lutjeharms, J.R.E., Beljaars, A.C.M., 2003. Underestimation of latent and sensible heat fluxes above the Agulhas Current in NCEP and ECMWF analyses. *J. Climate* 16, 776–782.
- Samelson, R.M., Skillingstad, E.D., Chelton, D.B., Esbensen, S.K., O'Neill, L.W., Thum, N., 2006. On the coupling of wind stress and sea surface temperature. *J. Climate* 19, 1557–1566.
- Sampe, T., 2005. Importance of midlatitude oceanic frontal zones for the general circulation of the extratropical troposphere. Ph.D. Dissertation. University of Tokyo, 108 pp., unpublished.
- Sampe, T., Xie, S.-P., 2007. Mapping high sea winds from space: a global climatology. *Bull. Am. Meteor. Soc.* 88, 1965–1978.
- Sanders, F., 1986. Explosive cyclogenesis in the west-central North Atlantic Ocean, 1981–84. Part I: composite structure and mean behavior. *Mon. Wea. Rev.* 114, 1781–1794.
- Sanders, F., Gyakum, J.R., 1980. Synoptic-dynamic climatology of the “Bomb”. *Mon. Wea. Rev.* 108, 1589–1606.
- Sasaki, H., Nonaka, M., 2006. Far-reaching Hawaiian Lee countercurrent driven by wind-stress curl induced by warm SST band along the current. *Geophys. Res. Lett.* 33, L13602, doi:10.1029/2006GL0265540.
- Scharroo, R., Smith, W.H.F., Lillibridge, J.L., 2005. Satellite altimetry and the intensification of Hurricane Katrina. *EOS Trans. Am. Geophys. Union* 86, 366.
- Scott, J.C., McDowall, A.L., 1990. Cross-frontal cold jets near Iceland: in-water, satellite infrared and Geosat altimeter data. *J. Geophys. Res.* 95, 18005–18014.
- Seo, H., Jochum, M., Murtugudde, R., Miller, A.J., 2006. Effect of ocean mesoscale variability on the mean state of tropical Atlantic climate. *Geophys. Res. Lett.* 33, L09606, doi:10.1029/2005GL0256651.
- Seo, H., Jochum, M., Murtugudde, R., Miller, A.J., Roads, J.O., 2007b. Feedback of tropical instability wave-induced atmospheric variability onto the ocean. *J. Climate* 20, 5842–5855.
- Seo, H., Miller, A.J., Roads, J.O., 2007a. The Scripps coupled ocean–atmosphere regional (SCOAR) model, with applications in the Eastern Pacific sector. *J. Climate* 20, 381–402.
- Shay, L.K., Goni, G.J., Black, P.G., 2000. Effects of a warm oceanic feature on Hurricane Opal. *Mon. Wea. Rev.* 128, 1366–1383.
- Shchepetkin, A.F., McWilliams, J.C., 2005. The regional oceanic modeling system (ROMS): a split-explicit, free-surface, topography-following coordinate oceanic model. *Ocean Modell.* 9, 347–404.
- Sikora, T.D., Young, G.S., Beal, R.C., Edson, J.B., 1995. Use of spaceborne synthetic aperture radar imagery of the sea surface in detecting the presence and structure of the convective marine atmospheric boundary layer. *Mon. Wea. Rev.* 123, 3623–3632.
- Singleton, A.T., Reason, C.J.C., 2006. Numerical studies of a severe rainfall event over the Eastern Cape coast of South Africa: sensitivity to sea surface temperature and topography. *Tellus* 58A, 355–367.
- Skamarock, W.C., Klemp, J.B., Dudhia, J., Gill, D.O., Barker, D.M., Wang, W., Powers, J.G., 2005. A description of the Advanced Research WRF Version 2. Technical note. National Center for Atmospheric Research, TN-468+STR. WWW page: <http://www.mmm.ucar.edu/wrf/users/docs/arw.v2.pdf>.
- Skillingstad, E.D., Vickers, D., Mahrt, L., Samelson, R., 2007. Effects of mesoscale sea surface temperature fronts on the marine atmospheric boundary layer. *Bound.-Layer Meteor.* 123, 219–237.
- Small, R.J., Xie, S.-P., Hafner, J., 2005a. Satellite observations of mesoscale ocean features and copropagating atmospheric surface fields in the tropical belt. *J. Geophys. Res.* 110, C02021, doi:10.1029/2004JC002598.
- Small, R.J., Xie, S.-P., Wang, Y., 2003. Numerical simulation of atmospheric response to Pacific tropical instability waves. *J. Climate* 16, 3723–3741.
- Small, R.J., Xie, S.-P., Wang, Y., Esbensen, S.K., Vickers, D., 2005b. Numerical simulation of boundary layer structure and cross-equatorial flow in the eastern Pacific. *J. Atmos. Sci.* 62, 1812–1830.
- Song, Q., Cornillon, P., Hara, T., 2006. Surface wind response to oceanic fronts. *J. Geophys. Res.* 111, C12006, doi:10.1029/2006JC003680.
- Song, Q., Hara, T., Cornillon, P., Friehe, C.A., 2004. A comparison between observations and MM5 simulations of the marine atmospheric boundary layer across a temperature front. *J. Atmos. Ocean. Tech.* 21, 170–178.
- Spall, M.A., 2007a. Midlatitude wind stress-sea surface temperature coupling in the vicinity of ocean fronts. *J. Climate* 20, 3785–3801.
- Spall, M.A., 2007b. Effect of sea surface temperature-wind stress coupling on baroclinic instability in the ocean. *J. Phys. Oceanogr.* 37, 1092–1097.
- Stammer, D., 1997. Global characteristics of ocean variability estimated from regional TOPEX/POSEIDON altimeter measurements. *J. Phys. Oceanogr.* 27, 1743–1769.
- Stommel, H., 1966. The Gulf Stream. A Physical and Dynamical Description. University of California Press, Berkeley and Los Angeles, USA, 248 pp.
- Stull, R.B., 1988. An introduction to boundary layer meteorology. Kluwer Academic Publishers, Dordrecht, The Netherlands, 670 pp.

- Sublette, M.S., Young, G.S., 1996. Warm-season effects of the Gulf Stream on mesoscale characteristics of the atmospheric boundary layer. *Mon. Wea. Rev.* 124, 653–667.
- Sweet, W., Fett, R., Kerling, J., La Violette, P., 1981. Air-sea interaction effects in the lower troposphere across the north wall of the Gulf Stream. *Mon. Wea. Rev.* 109, 1042–1052.
- Taguchi, B., Xie, S.-P., Schneider, N., Nonaka, M., Sasaki, H., Sasai, Y., 2007. Decadal variability of the Kuroshio extension: observations and an eddy-resolving model hindcast. *J. Climate* 20, 2357–2377.
- Thum, N., Esbensen, S.K., Chelton, D.B., McPhaden, M.J., 2002. Air-sea heat exchange along the northern sea surface temperature front in the eastern tropical Pacific. *J. Climate* 15, 3361–3378.
- Tokinaga, H., Tanimoto, Y., Nonaka, M., Taguchi, B., Fukamachi, T., Xie, S.-P., Nakamura, H., Watanabe, T., Yasuda, I., 2006. Atmospheric sounding over the winter Kuroshio Extension: Effect of surface stability on atmospheric boundary layer structure. *Geophys. Res. Lett.* 33, L04703, doi:10.1029/2005GL025102.
- Tokinaga, H., Tanimoto, Y., Xie, S.-P., 2005. SST-induced surface wind variations over the Brazil-Malvinas confluence: satellite and in situ observations. *J. Climate* 18, 3470–3482.
- Tomczak, M., Godfrey, J.S., 1994. Regional Oceanography: An Introduction. Pergamon/Elsevier, New York, USA, 422 pp.
- Trasviña, A., Barton, E., Brown, J., Velez, H., Kosro, P., Smith, R., 1995. Offshore wind forcing in the Gulf of Tehuantepec, Mexico: the asymmetric circulation. *J. Geophys. Res.* 100, 20649–20663.
- Trunk, T.J., Bosart, L.F., 1990. Mean radar echo characteristics during project GALE. *Mon. Wea. Rev.* 118, 459–469.
- Vecchi, G.A., Xie, S.-P., Fischer, A., 2004. Ocean-atmosphere covariability in the western Arabian Sea. *J. Climate* 17, 1213–1224.
- Venkatram, A., 1977. A model of internal boundary layer development. *Bound.-Layer Meteor.* 11, 419–437.
- Vihma, T., Launiainen, J., Krause, G., 1991. On the air-sea interaction in areas of thermal marine fronts in the Greenland Sea. *Atmos. Ocean* 29, 596–610.
- Vihma, T., Uotila, J., Launiainen, J., 1998. Air-sea interaction over a thermal marine front in the Denmark Strait. *J. Geophys. Res.* 103, 27665–27678.
- Wai, M.M.-K., Stage, S.A., 1989. Dynamical analyses of marine atmospheric boundary layer structure near the Gulf Stream oceanic front. *Quart. J. R. Meteor. Soc.* 115, 29–44.
- Wallace, J.M., Mitchell, T.P., Deser, C., 1989. The influence of sea surface temperature on surface wind in the eastern equatorial Pacific: seasonal and interannual variability. *J. Climate* 2, 1492–1499.
- Wang, Y., Sen, O.L., Wang, B., 2003. A highly resolved regional climate model (IPRC-RegCM) and its simulation of the 1998 severe precipitation event over China. Part I: Model description and verification of simulation. *J. Climate* 16, 1721–1738.
- Warner, T.T., Lakhtakia, M.N., Doyle, J.D., Pearson, R.A., 1990. Marine atmospheric boundary layer circulations forced by Gulf Stream sea surface temperature gradients. *Mon. Wea. Rev.* 118, 309–323.
- Wayland, R.J., Raman, S., 1989. Mean and turbulent structure of a baroclinic marine boundary layer during the 28 January 1986 cold-air outbreak (GALE 86). *Bound.-Layer Meteor.* 48, 227–254.
- Weissman, D.E., Thompson, T.W., Legeckis, R., 1980. Modulation of sea surface radar cross section by surface stress: Wind speed and temperature effects across the Gulf Stream. *J. Geophys. Res.* 85, 5032–5042.
- Wentz, F.J., Gentemann, C., Smith, D., Chelton, D., 2000. Satellite measurements of sea surface temperature through clouds. *Science* 288, 847–850.
- White, W.B., Annis, J.L., 2003. Coupling of extratropical mesoscale eddies in the ocean to westerly winds in the atmospheric boundary layer. *J. Phys. Oceanogr.* 33, 1095–1107.
- Worthington, L.V., 1977. Intensification of the Gulf Stream after the winter of 1976–77. *Nature* 270, 415–417.
- Wu, Q., Bowman, K., 2007. Multiyear satellite observations of the atmospheric response to Atlantic tropical instability waves. *J. Geophys. Res.* 112, D19104, doi:10.1029/2007JD008627.
- Xie, S.-P., Ishiwatari, M., Hashizume, H., Takeuchi, K., 1998. Coupled ocean-atmospheric waves on the equatorial front. *Geophys. Res. Lett.* 25, 3863–3866.
- Xie, S.-P., 2004. Satellite observations of cool ocean-atmosphere interaction. *Bull. Am. Meteor. Soc.* 85, 195–208.
- Xie, S.-P., Chang, C.-S., Xie, Q., Wang, D., 2007a. Intraseasonal variability in the summer South China Sea: The wind jet, cold filament, and recirculations. *J. Geophys. Res.* 112, C10008, doi:10.1029/2007JC004238.
- Xie, S.-P., Hafner, J., Tanimoto, Y., Liu, W.T., Tokinaga, H., Xu, H., 2002. Bathymetric effect on the winter sea surface temperature and climate of the Yellow and East China Seas. *Geophys. Res. Lett.* 29, 2228, doi:10.1029/2002GL015884.
- Xie, S.-P., Miyama, T., Wang, Y., Xu, H., deSzoeke, S.P., Small, R.J.O., Richards, K.J., Mochizuki, T., Awaji, T., 2007b. A regional ocean-atmosphere model for eastern Pacific climate: towards reducing tropical biases. *J. Climate* 20, 1504–1522.
- Xue, H., Bane, J.M., Goodman, L.M., 1995. Modification of the Gulf Stream through strong air-sea interactions in winter: observations and numerical simulations. *J. Phys. Oceanogr.* 25, 533–557.
- Xue, H., Pan, Z., Bane, J.M., 2000. A coupled atmosphere-ocean study of air-sea interactions during a cold air outbreak over the Gulf Stream. *Mon. Wea. Rev.* 128, 973–996.
- Yoder, J.A., Ackleson, S.G., Barber, R.T., Flament, P., Balch, W.M., 1994. A line in the sea. *Nature* 371, 689–692.
- Young, G.S., Sikora, T.D., 2003. Mesoscale stratocumulus bands caused by Gulf Stream meanders. *Mon. Wea. Rev.* 131, 2177–2191.
- Zebiak, S.E., 1986. Atmospheric convergence feedback in a simple model for El-Niño. *Mon. Wea. Rev.* 114, 1263–1271.